Taylor & Francis
Taylor & Francis Group

Applied Earth Science

Transactions of the Institutions of Mining and Metallurgy

ISSN: (Print) (Online) Journal homepage: https://www.tandfonline.com/loi/yaes21

The geology and geochemistry of the Rhyacian Josephine gold deposit, Northwest Ghana

Fuseini Atanga, Prince Ofori Amponsah, Samuel Nunoo, Daniel Kwayisi, Eric Dominic Forson, Thomas Mba Akabzaa & Prosper Mckenzie Nude

To cite this article: Fuseini Atanga, Prince Ofori Amponsah, Samuel Nunoo, Daniel Kwayisi, Eric Dominic Forson, Thomas Mba Akabzaa & Prosper Mckenzie Nude (29 Sep 2023): The geology and geochemistry of the Rhyacian Josephine gold deposit, Northwest Ghana, Applied Earth Science, DOI: 10.1080/25726838.2023.2260583

To link to this article: https://doi.org/10.1080/25726838.2023.2260583

APPLIED EARTH SCIENCE (TRANS. INST. MIN. METALL. B)
https://doi.org/10.1080/25726838.2023.2260583

RESEARCH ARTICLE

The geology and geochemistry of the Rhyacian Josephine gold deposit, Northwest Ghana

Fuseini Atanga[a], Prince Ofori Amponsah [a], Samuel Nunoo[a], Daniel Kwayisi[a], Eric Dominic Forson[b], Thomas Mba Akabzaa[a] and Prosper Mckenzie Nude[a]

[a]School of Physical and Mathematical Sciences, Department of Earth Science, University of Ghana, Legon-Accra, Ghana; [b]School of Physical and Mathematical Sciences, Department of Physics, University of Ghana, Legon-Accra, Ghana

ABSTRACT

This paper focuses on the geology and geochemistry of the Rhyacian Josephine gold deposit in northwestern Ghana, where gold is primarily hosted in quartzites, with other lithologies observed, including granitoids, mafic intrusions, and gneisses. Four deformational events, D_{JO0}, D_{JO1}, D_{JO2}, and D_{JO3}, are observed. D_{JO0} is synonymous with the primary preserved sedimentary crossbedding in the quarzitic rocks. Gold mineralization within the deposit is mainly associated with the D_{JO1} NNW-trending dextral and steeply dipping sinusoidal shear zone. Gold occurs primarily as free gold and invisible gold within the lattices of the disseminated arsenopyrite along the shear foliation planes of the host rock. The ore body geometry is 15–40 m wide and strikes 800 m in the NNW direction. Silicification, sericitization, chloritization, and sulphidation are the main alteration assemblages associated with the gold mineralization zones within the Josephine deposit. Pathfinder elements for gold are stibnite, tellurium, sulphur, copper, silver, and Lead.

ARTICLE HISTORY
Received 13 June 2023
Revised 10 August 2023
Accepted 12 September 2023

KEYWORDS
Deformation; alteration; mineralisation; ore body; Josephine deposit

Introduction

Northwest Ghana is increasingly becoming an important metallogenic province for gold, due to the discovery of various gold camps by Azumah Resources Limited, namely, the Duri-Basabli, Doggo-Yagha, Kunche-Bepkong, Butele-Dorimon (Amponsah et al. 2016b; Nunoo et al. 2022a, 2022b; Amponsah and Forson 2023; Forson and Amponsah 2023), Josephine-Manwe (Azumah Resources 2016), Julie (Amponsah et al. 2015; Amponsah et al. 2016a), Kjersti and Collette gold camps (Figure 1). Kunche, Bepkong and Julie gold camps have been developed into a ready to mine deposits. To date, Azumah Resources Limited has discovered 2.8 million ounces of gold and is still discovering more due to ongoing systematic scientific mineral exploration works (Ibaera Capital 2022). This metallogenic province is important for economic and scientific reasons. It is therefore imperative to understand the less-known deposits in this metallogenic region as means of discovering new targets and increase the gold inventory in the area. The results will also serve as a useful guide for further exploration of gold in green field areas in this metallogenic province. Thus, understanding the geology and geochemistry of the Josephine deposit which is one of the less-known deposits, with inferred Au resources of 69,000 oz; (Azumah Resources 2016) and owned by Azumah Resources in NW Ghana can be considered as critical in the development and advancement of the deposit as well as the gold mineralisation systematics in the province.

The Josephine deposit is located in the Paleoproterozoic Birimian terrane and gold mineralisation associated with this terrane is linked to orogenic-type deposits (Milési et al. 1992; Béziat et al. 2008; Hammond et al. 2011; Lawrence et al. 2013; Treloar et al. 2015; Augustin and Gaboury 2019; Tourigny et al. 2019). Thus, the deposit formed in an accretionary and collisional settings (Abouchami et al. 1990; Leube et al. 1990; Baratoux et al. 2011; Grenholm et al. 2019) and found within rocks that have experienced varying degrees of metamorphism and tectonic deformation (Groves et al. 1998; Goldfarb et al. 2001; Groves et al. 2020). The Birimian is also characterised by volcanic activity and analogous to an archipelago-like setting with arcs and basins (Grenholm et al. 2019). The primary objective of this research is to provide details of the geological aspects of the Josephine gold deposit in NW Ghana, the alteration geochemistry, and the style of the gold mineralisation. The results will be compared to other deposits studied in NW Ghana. This will in turn aid in the exploration and targeting process of newer green fields in NW Ghana.

CONTACT Prince Ofori Amponsah pamponsah@ug.edu.gh School of Physical and Mathematical Sciences, Department of Earth Science, University of Ghana, P.O. Box LG 58, Legon-Accra, Ghana

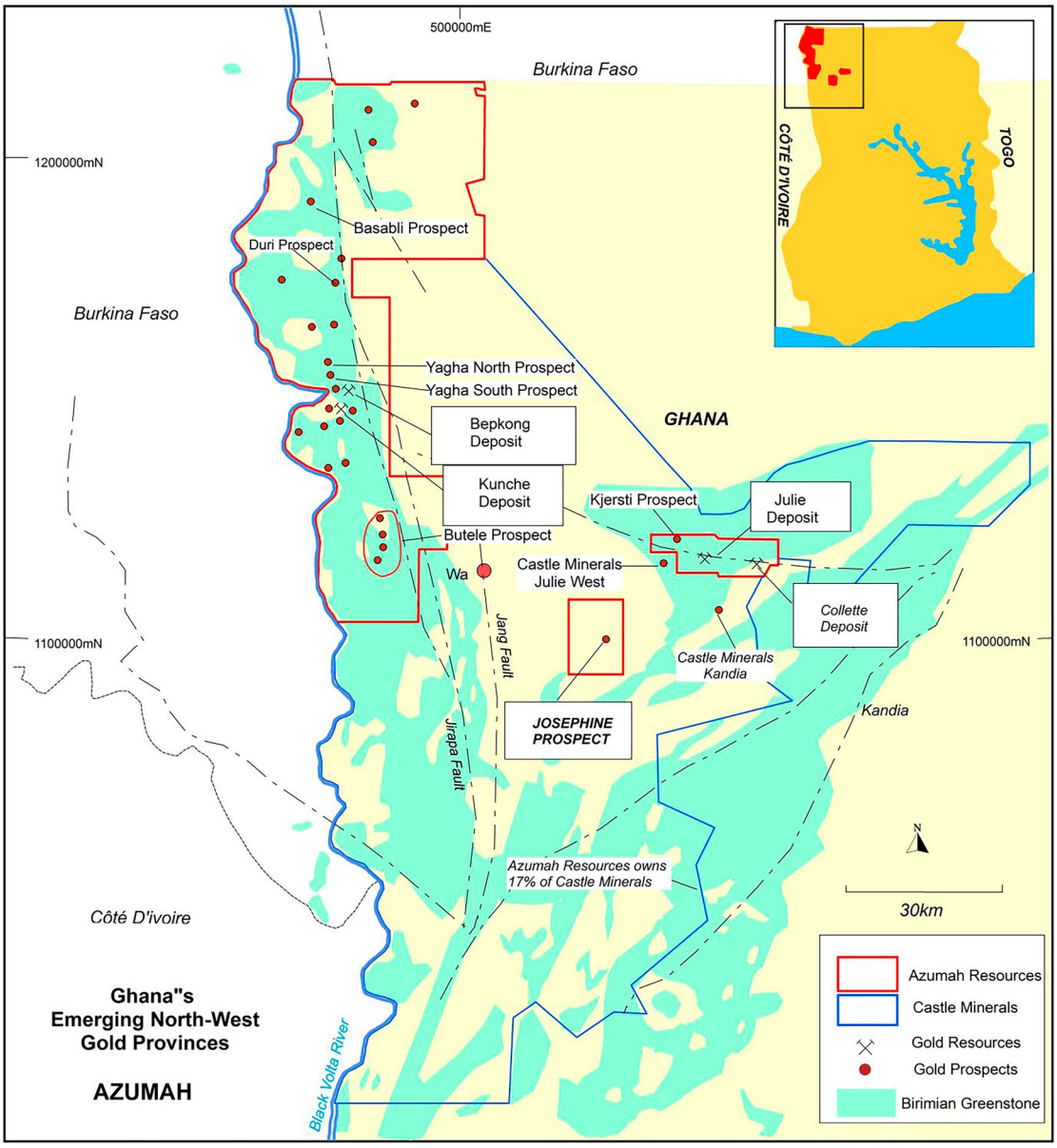

Figure 1. Map of the northern part of Ghana showing Azumah permits which includes the Josephine PL (the red rectangular box; (a), and their location on the insert Ghana map (b) (after Azumah resource limited, 2015).

Geological setting

The Eburnean orogeny is characterised as a succession of diverse stages of magmatic activities, tectonic movements, and metamorphic processes that resulted in the creation and establishment of the Paleoproterozoic Birimian region situated to the east of the Archaean-age Kenema-Man region within the southern part of the West African Craton (sWAC; Figure 2) (Jessell et al. 2012; Salvi et al. 2016; Diatta et al. 2017; McFarlane et al. 2019; Forson et al. 2020, 2021; Masurel et al. 2022; Amponsah et al. 2023). The Birimian straddles countries like Mali, Ivory Coast, Ghana, Niger, Senegal and Burkina Faso. Architecturally, the Birimian in Ghana is made up of five northeast-southwest trending greenstone belts (Amponsah 2012; Perrouty et al. 2012; Nunoo et al. 2016; Forson et al. 2022, 2023; Agra et al. 2023) as well as a north–south oriented greenstone belt (Amponsah et al. 2015; Amponsah et al. 2016a, 2016b; Asiedu et al. 2019; Sapah et al. 2020; Nunoo et al. 2022a, 2022b), with intervening basins (Amponsah 2016a; Davis et al. 1994). The Wa-Lawra belt in Ghana, which runs in a north–south direction, forms a segment of the broader Boromo belt that stretches northward into Burkina Faso (Baratoux et al. 2011; Block et al. 2016; Feng et al. 2018, 2019).

Block et al. (2016) described the geology of northwest Ghana to be made up of two distinct cratonic blocks (the western block dominated by a north–south structural trend and the eastern block dominated by a northeast-southwest structural trend) that converge within a tangential intersection in northwest Ghana. The western block, influenced by a north–south structural alignment, is characterised by the presence of the Wa-Lawra belt. The eastern

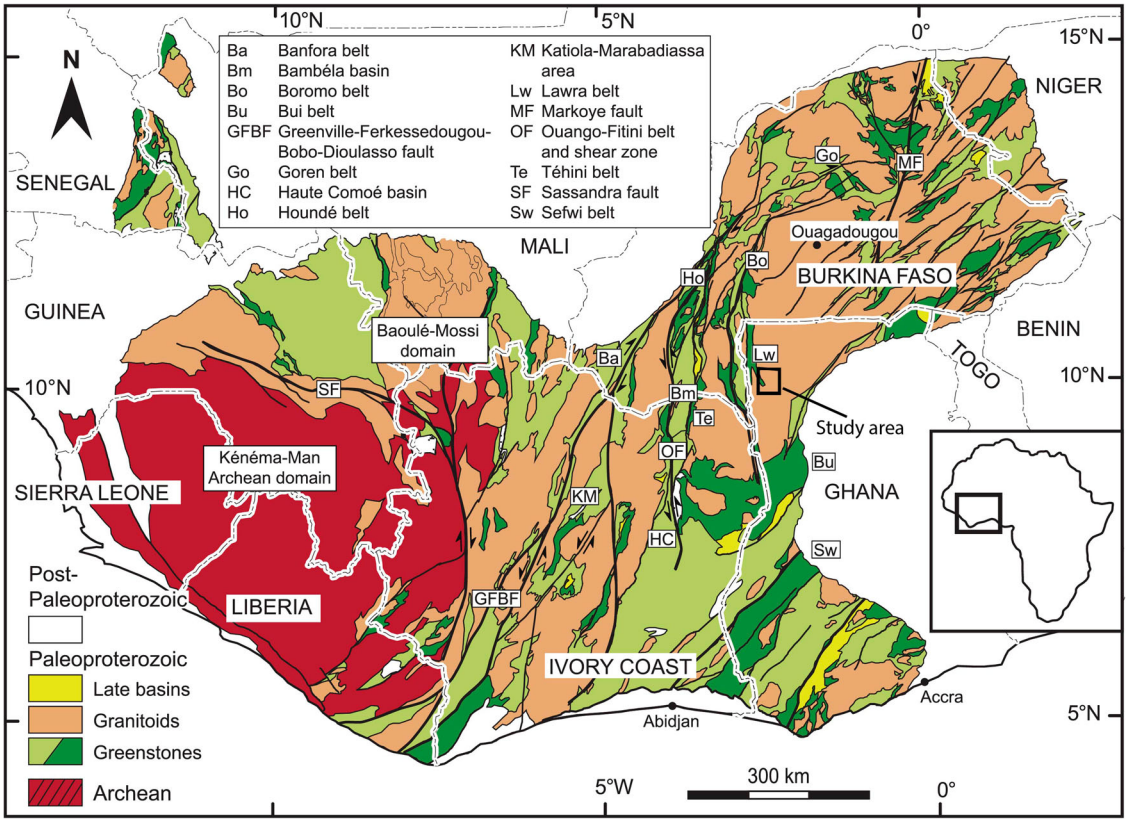

Figure 2. Simplified map of Africa and simplified geological map of the Leo-Man shield Also shown is an insert of the map of Africa showing the location of the Birimian domain of the West African Craton (modified after Milési et al. 2004).

block is made up of three distinct areas: Koudougou-Tumu terrane, Julie belt, and Bole-Bulenga terrane. (Figure 3). The Wa-Lawra belt consists of sediments, including greywackes, volcano-sediments, shales, greywacke, and volcano-sediments, that have undergone regional metamorphism and deformation around 2139 ± 2 Ma (Amponsah et al. 2015; Block et al. 2015) and early syntectonic (2212 ± 1 Ma to 2153 ± 4 Ma); (Duodu 2009; Sakyi et al. 2014) granitoid intrusions. Intruding these rocks are late 2104 ± 4 Ma granitoids, that appear to be relatively undeformed.

The Koudougou-Tumu terrane is composed of granitoids as well as high-grade gneisses formed approximately 2187 ± 3 Ma, is positioned adjacent to the Wa-Lawra belt through the north-northwest trending Jirapa and Jang faults (Duodu 2009; Sakyi et al. 2014) and gneisses as well as gabbro with approximate ages between 2162 ± 1 Ma and 2134 Ma gneisses. These rocks were intruded by 2128 Ma late granite with porphyritic texture. (Duodu 2009; Amponsah et al. 2015) and amphibolite metamorphic facies (Block et al. 2016).

The Julie belt as well as the Bole-Bulenga domain are situated southwards of the Koudougou-Tumu terrane. Within the Julie belt, there are metamorphosed basalts, rhyolite volcano-sedimentary rocks, and TTGs (tonalite-trondhjemite-granodiorite) exhibiting granodioritic characteristics, all of which have undergone metamorphism to the greenschist facies (Amponsah et al. 2015; Block et al. 2015) determined an age of 2129 ± 7 Ma in the volcaniclastics rocks (Agyei-Duodu et al. 2009). Bole-Bulenga consist mainly of high-grade paragneisses are intruded by orthogneisses, with crystallization ages spanning from 2195Ma to 2135 Ma. Towards the south, both Bole-Bulenga domain and the Julie belt are adjacent to the Bole-Nangodi shear zone. This crustal-scale shear zone extends in a northeast-southwest direction along the boundary of the Wa-Lawra belt and the Koudougou-Tumu domain (Block et al. 2015). The Bole-Nangondi belt consists mainly of granites, shales, volcaniclastics, and gneisses that have ages of crystallization varying from around 2196 ± 1 Ma to 2118 ± 3 Ma (Duodu 2009; De Kock et al. 2011).

Baratoux et al. (2011) and Block et al. (2016) described a polycyclic structural setting for NW Ghana. These authors recognised and defined seven deformational events (denoted D1 to D7). Deformation episodes D1-D3 took place between 2144 and 2110 Ma. D1 is characterised by a north–south compressive event resulting in the east–west trending nappes of the Julie belt. D2 is typified by a gravitational collapse responsible for the north–south extension fabrics which essentially brought together the low as well as the high-grade rocks. D3 and D4 are

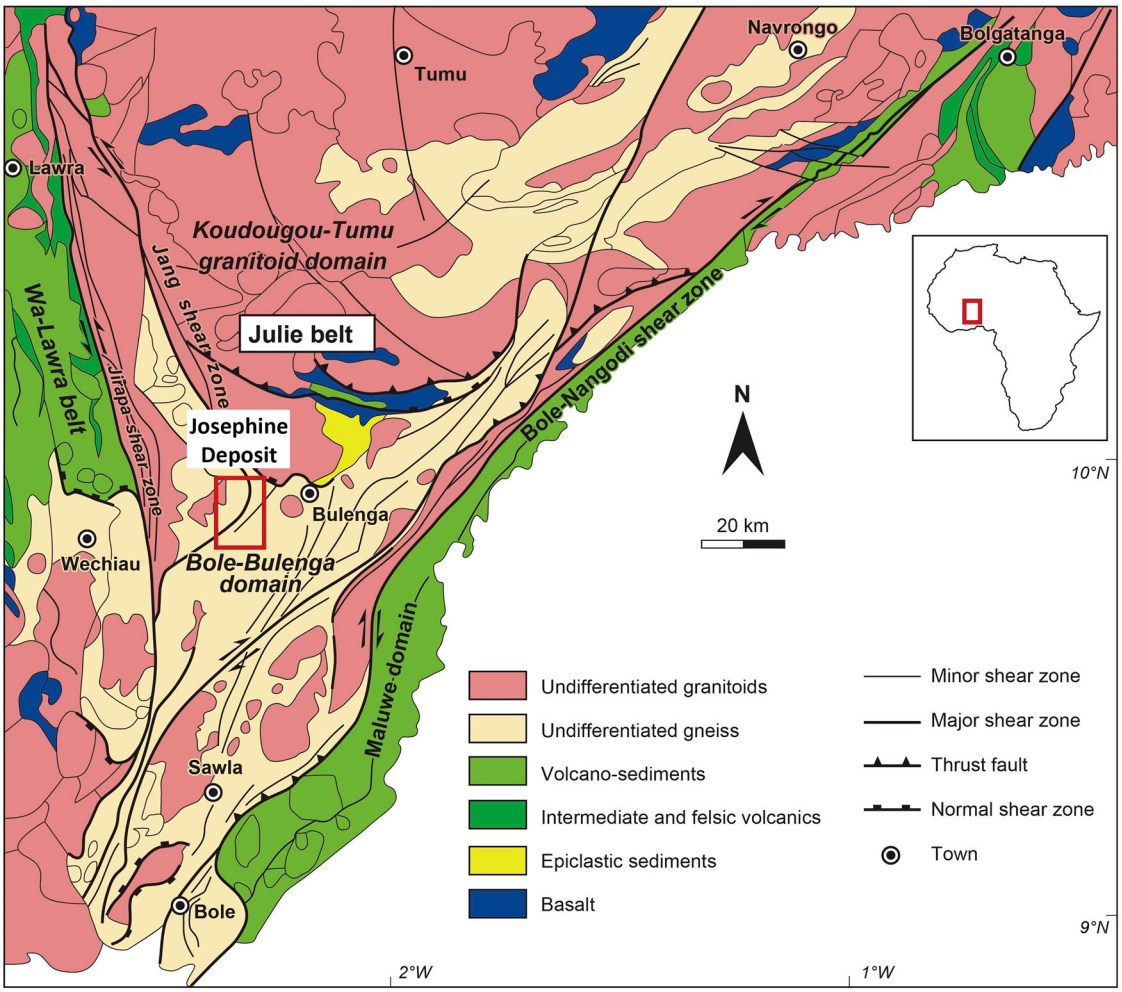

Figure 3. Simplified regional lithological map of the Paleoproterozoic Birimian of Northwest Ghana (modified after Block et al. 2015). Shown in the red insert is the study area.

characterised by a north–south structural stretching with localised dilatational jogs. D5 is associated with the reactivation of inherited structures that resulted in varying generations of shear zones. The late E-W brittle deformation in the region is indicative of a D6-D7 deformational episode.

Methodology

To provide a comprehensive account of the geology and alteration geochemistry of the Josephine deposit, a systematic geological field mapping was conducted at a scale of 1:50,000. This mapping considered various factors such as lithology, ore minerals, alterations, tectonic and structural characteristics including folds, foliation, lineation, kinematic indicators, and other relevant petrofabric parameters. Borehole data including reverse circulation (RC) data and diamond core data (DD) were also logged.

The samples collected from the field mapping work were first analysed in hand specimen and then microscopically from standard thin section with the Leica DM750P petrographic microscope a fitted with AmScope Digital camera at the Department of Earth Science, University of Ghana. Mineralised samples analysed with a scanning electron microscope (Zeiss EVO MA15 SEM) together with an energy dispersive X-ray spectrometer (Bruker Nano GmbH) and an XFlash Detector 610M at the geological engineering laboratory, University of Mines and Technology, Tarkwa, Ghana.

Also, 10 samples (5 altered and 5 unaltered) were selected for the purpose of whole-rock geochemical analysis at the ALS laboratory in Canada. The result was used to evaluate quantitatively the chemical losses and gains during the alteration process in the Josephine deposit. The composition of major oxides and trace-elements were used for the evaluation (Isocon analyses after Grant (1986)). The Grant (1986) isocon technique assesses substantial changes in composition, mass, and volume. The mass, volume and compositional variations were calculated using the EASY-GRESGRANT MS-Excel sheet and procedures as described in Lopez-Moro (2012).

The geological mapping data were integrated with aeromagnetic and electromagnetic data to produce maps for the study area (Figure 5). The different structural plots were generated using the stereo-net

software (version 11.50) (Cardozo and Allmendinger 2013).

Results

Deposit scale geology

This covers rocks that characterise the Josephine deposit, the deformational episodes experienced by the lithologies, alteration haloes, ore geometry and characterisation. Other aspects include ore mineralogy and mass-balance considerations from isocon analysis. Such details are valuable to establish the structural linkage to gold mineralisation, the host sulphide mineral, and the associated alteration. Rocks encountered on the Josephine deposit are granitoids, quartzites, dolerite sill and gneisses.

Petrography

Petrographically, the granitoids can be categorised into three types. These are granodiorite, granite, and diorite. The granodiorite is phaneritic, leucocratic and mineralogically composed of plagioclase (35%), orthoclase (20%), and quartz (20%), with a minor amount of magnetite as accessory minerals (Figure 4(a)). Microscopically, the granodiorite exhibits holocrystalline and hypidiomorphic-granular texture (Figure 4(b)). The granite is also phaneritic, leucocratic and composed of quartz (65%), plagioclase (20%), orthoclase (10%), muscovite and sulphides as accessory mineral. They are also holocrystalline and possess hypidiomorphic-granular textures (Figure 4(c) and (d)). The dolerite is mesocratic, has a phaneritic texture and composed of plagioclase (30%), quartz (15%), hornblende (20%), biotite (15%) with pyrite and muscovite as accessory mineral. They exhibit shearing and veining. In thin section, the texture of the diorite is allotriomorphic, granular, and it is also holocrystalline (Figure 4(e) and (f)).

The quartzites are grey, medium grained, contain preserved tabular cross stratification and where there is intense shearing, they exhibit schistose textures. Mineralogically, the quartzite contains quartz (95%), k-feldspar (2%), and traces of plagioclase, biotite, and chlorite. Where the rocks have experienced intense shearing, biotite and muscovite tends to grow along the schistose planes. In thin section, the quartzite shows varying textures including porphyroblastic, poikiloblastic and schistose texture (Figure 4(g) and (h)).

The dolerites are dark green in colour, fine to medium grained, mostly sheared, highly magnetic and composed of plagioclase (40%), amphibole (15%), pyroxene (20%) and chlorite (4%) with quartz (15%) and magnetite as accessory minerals. Quartzo-feldspathic veining was also observed in the dolerite. Microtextural analysis revealed that the dolerite is hypocrystalline and sheared, as exemplified by the elongation of minerals (Figure 4(i) and (j)), with plagioclase showing sub-ophitic and lath-shaped textures.

The gneisses have alternating leucocratic and melanocratic colours as a result of obvious typomorphic textures. They are coarse grained and generally composed of biotite (15%), plagioclase (20%), K-feldspar (25%), quartz (30%), amphibole (3%), with minor chlorite (2%) and magnetite (2%) as accessory mineral. Under thin section, biotite appears elongated and is surrounded by plagioclase (Figure 4(k) and (l)).

Structural features and deformation

The structural features of rocks of the Josephine deposit (Figure 5) are interpreted to be indicative of four deformational regimes (D_{JO0}, D_{JO1}, D_{JO2} and D_{JO3}). The deformation represents a progressive brittle-ductile deformation.

DJO_0 deformational regime

Within the Josephine deposit, D_{JO0} is connected to a S_{JO0} that exhibits a shallow-to-steep dipping pattern. This S_{JO0} is characterised by the presence of preserved planar/tabular cross-stratigraphic layering found specifically within the quartzites. The quartzites are observed within the central portion of the study area (Manwe). The general bedding (S_{JO0}) trend is NW-SE with steep dips in the NE direction as shown in the field photograph and Schmidt plot in Figure 6(a) and (b) respectively below.

DJO_1 deformational regime

D_{JO1} deformational event is the dominant deformational event in the study area. It has affected almost all the rocks within the study area. D_{JO1} is linked to steeper NNW trending 40 km shear zone with a general NE-dipping sequence. This shear zone is defined by a right-stepping relay or dilatational jogs with a dextral sense of movement as well as right lateral faults (Riedel shear) that inclines gently into the main S_{JO1} shear foliation. This deformational regime is also linked with a shallow to steeply dipping S_{JO1} shear foliation known as right-stepping relay or sinusoidal shear bend (dilatational jogs), parallel to the S_{JO0} bedding with lineation (L_{1JO1}) plunging down-dip (Figure 7(a) and (b)). This shallow-steep dips on the shear zone defines a hanging and a foot wall sequence on the shear zone. The steep dips are the footwall, and the shallow dips are the hanging wall. S_{JO1} foliation has a top-to-the-NE kinematic indicators with down-dip plunging lineation. S_{JO1} shear foliation is defined by the axial planes of the F_{JO1} isoclinal folds striking in the NW-SE direction with steep dips to the NE direction (Figure 7(c) and (d)).

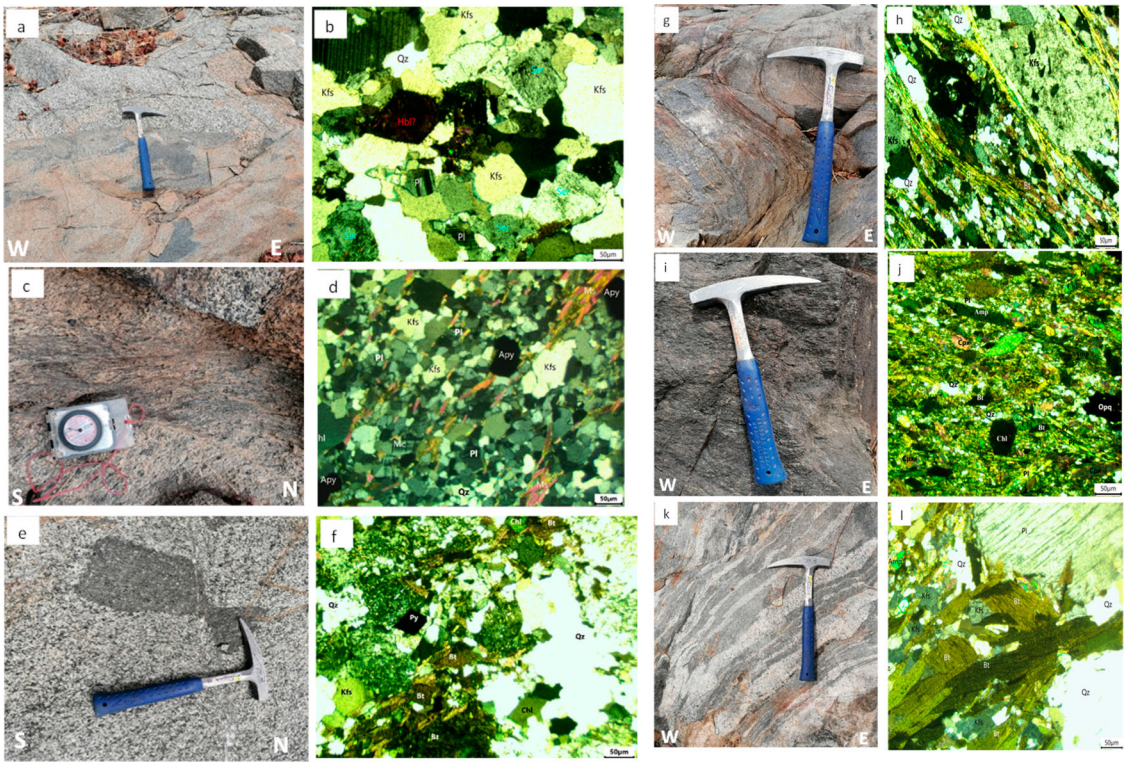

Figure 4. Field photos and corresponding photomicrographs of the Josephine deposit. (a and b) field photograph and photomicrograph of granodiorite showing hypidiomorphic-granular texture (cross polars) (c and d) field photograph and photomicrograph of granite (e and f) field photograph and photomicrograph of diorite (g and h) field photograph and photomicrograph showing strongly folded quartzite and porphyroblastic and poikiloblastic texture (cross polars) in quartzite respectively (i) field photograph of sheared dolerite, (j) photomicrograph of dolerite showing mineral elongation, indicative of shearing (cross polars), (k) field photograph of gneiss, (l) photomicrograph of gneiss (cross polars). Qz = quartz, Pl = plagioclase, Amp = amphibole, Kfs = K-feldspar, Bt = biotite, Pl = plagioclase, Px = pyroxene, Cpx = Clinopyroxene, Opx = Orthopyroxene, Chl = chlorite, Bt = biotite, Opq = opaque mineral, Apy = arsenopyrite, Py = pyrite, Hbl = hornblende, ms = microcline, and Ser = sericite. Mineral abbreviation is from Whitney and Evans (2010).

D_{JO2} deformational regime

D_{JO2} is associated to a NE-SW striking foliation (S_{JO2}; Figure 8(a) and (b)) whose dips ranges from 40° to 70° to the north-west and has a stretching lineation (L_{JO2}) trending NE-SW ($L_{JO2,}$ plunging to N250-350) which plunges (40-70°) down-dip. D_{JO2} is also defined by F_{JO2} open folds (Figure 8(a)). These could be seen in the meta-sedimentary rocks and granitoid intrusions. In the field, there is no observable overprinting relationships between D_{JO1} and D_{JO2} structures.

D_{JO3} deformational regime

The final stage of deformation D_{JO3} in the Josephine deposit is a brittle-ductile deformation which is associated with NNE-SSW S_{JO3} foliation (schistose cleavage), and dextral faulting (Figure 9(a) and (b)). Within the southern part of the study area, where high-grade metamorphic rocks such as garnetiferous quarzitic schist are present, S_{JO3} develops a pervasive foliation that aligns with ptygmatic F_{JO3} folds (see Figure 10 (a) and (b)). D_{JO3} is linked to an overlying metamorphic event characterised by amphibolite facies conditions. The fabrics, structural features, and isograds formed during D_{JO1} and D_{JO2} are subsequently modified by the deformation associated with D_{JO3}, indicating a consistent E-W directed horizontal contraction. In the northwest portion of the Josephine deposits, E-W oriented spaced cleavages have been observed within the granitoid (refer to Figure 10(d)).

Alteration

In the Josephine gold deposit, mineral alteration could be observed in both outcrops and drill cores. The diagnostic features of the altered zone which make it easily distinguishable from the unaltered zone is the bleaching of the rock (due to the intense silicification associated with the mineralised zone) as well as its mineral constituents.

Typically, some altered rocks tend to be greenish in colour and very hard. The mineral assemblage linked to the altered (mineralised) zone include chlorite + sulphides + sericite + quartz (silicification) (Figure 11 and 12). These alteration assemblages bleach the rock giving it an overall light greenish colouration. Minerals such as feldspars and micas also alter into sericite (sericitization). The sulphides present in the altered zone are arsenopyrite, pyrite, and chalcopyrite, with the arsenopyrite being dominant (usually 3-5% intensity within the mineralised zone) and exist as disseminated grains.

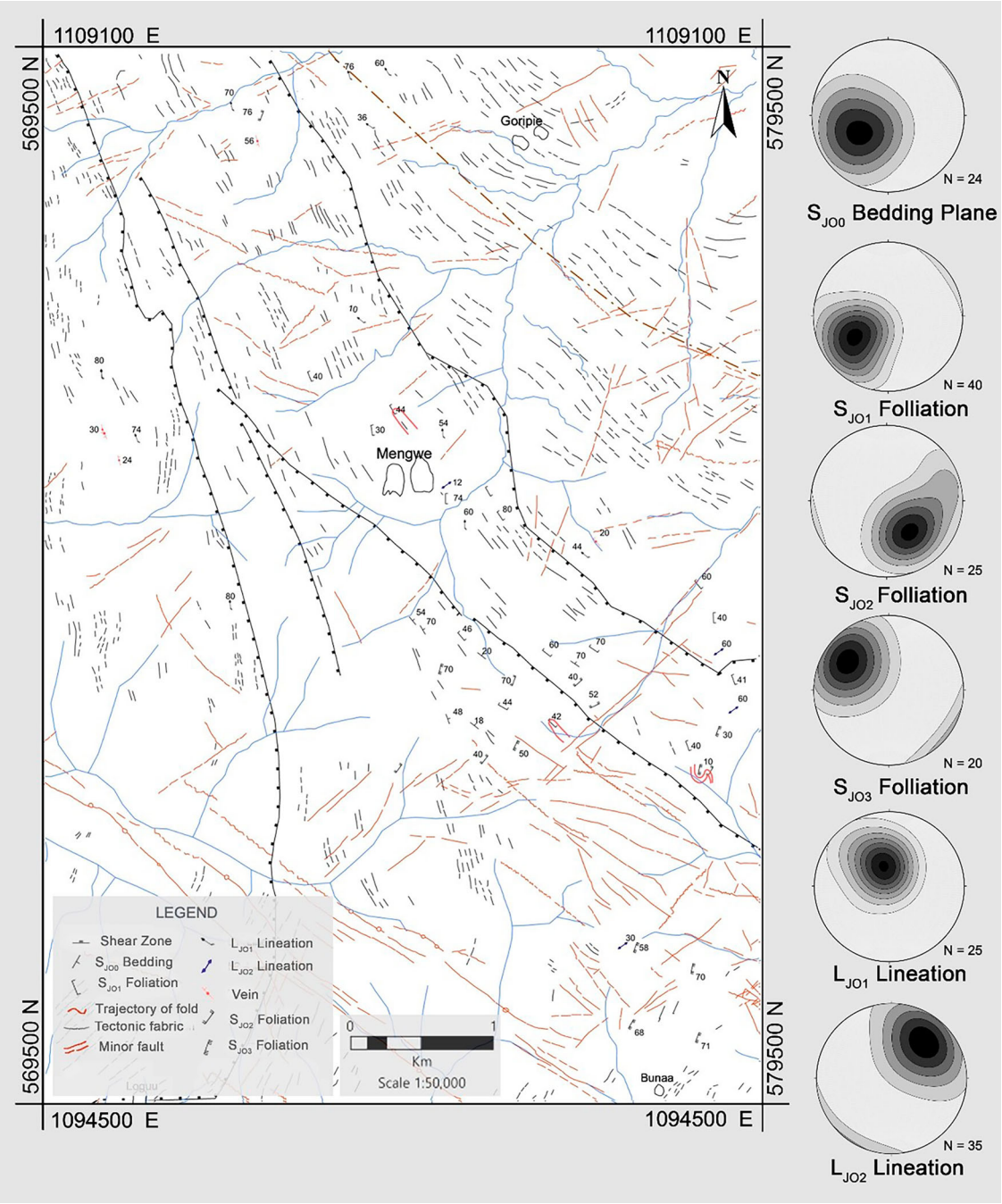

Figure 5. Simplified structural map of the Josephine deposit compiled from field structural measurements and structural fabric interpreted from aeromagnetic and electromagnetic geophysical data. Inserts are lower hemisphere stereographic projection for poles of the different deformational generations of foliation and lineaments.

Ore body geometry and characteristic

The orebody within the Josephine deposit is generally steeper, associated with NNW (clockwise) trending S_{JO1} shear zone within a general NE-dipping sequence. This is interpreted as a right-stepping relay or sinusoidal shear bend. The mineralised zone is about 15 to 40 m wide and 800 m long. It occurs within a 20–120 m thick alteration zone (Figure 12). The alteration mineral assemblage responsible for the mineralisation is quartz + chlorite + sericite + sulphide while alteration mineral assemblage of chlorite + hematite + sericite + magnetite appears to be ubiquitous across the whole study area.

The mineralisation observed at the Josephine deposit does not exhibit significant veining. Instead, there are minor occurrences of stringers and grey quartz veins in the drill core, which appear to have formed prior to the main stages of deformation and metamorphism.

Ore mineralogy

Analysing the texture of sulphide minerals plays a crucial role in obtaining significant information and insights regarding the source, history, and feasibility of deposits, as well as identifying potential challenges

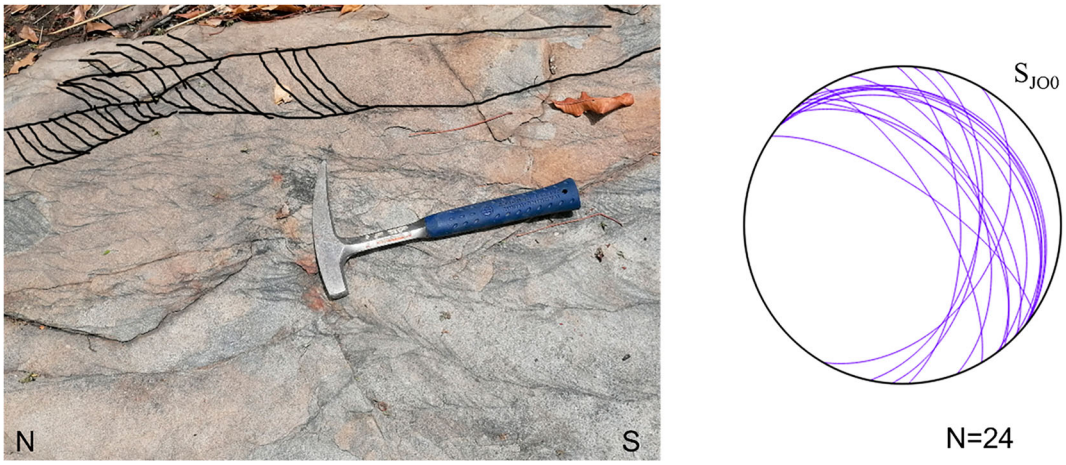

Figure 6. Field photographs and stereoplots showing structures in Josephine deposit. (a) Field photograph illustrating preserved sedimentary layering (cross bedding) and (b) an inserted Schmidt plot showing the general trend of the beds.

in mineral processing. In the Josephine deposit, quartzite is the only mineralised rock. From the ore petrographic analysis of sulphides in the quartzites, it is observed that disseminated arsenopyrite (Figure 13 (a)), chalcopyrite and pyrite (sulphides) were observed in the Josephine deposit with arsenopyrite being the only ore bearing sulphide. They occur along the foliations in the altered rocks and are associated with the silicified zones. Arsenopyrite is the most dominant and frequently occurring sulphide. It is typically coarse grained, shows zoning, whitish in colour (SEM images), euhedral and has a rhombic crystal shape. Chalcopyrite on the other hand grows on the arsenopyrite (Figure 13(c)).

By combining SEM image analysis, field observation, and petrographic analysis, it has been determined that the presence of mineralisation of gold in the Josephine deposit is closely linked to the occurrence of arsenopyrite. The gold is observed as disseminated inclusions within the arsenopyrite. (Figure 13(b,d)).

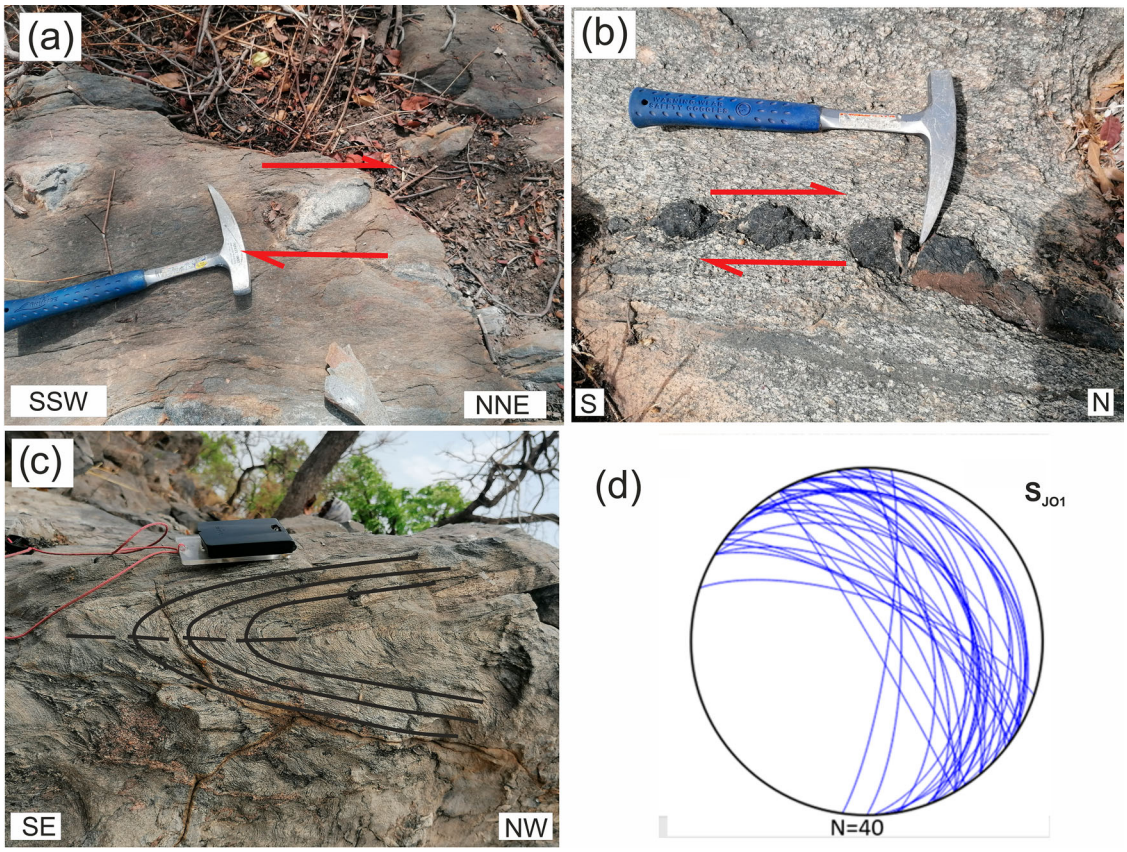

Figure 7. Field photographs and stereoplots showing structures in Josephine deposit. (a, b) field photographs showing S_{JO1} foliation and boudins indicating the top-to-the-NE kinematic indicator and dextral sense of movement (c) F_{JO1} isoclinal folds defining the S_{JO1} foliation and (d) an inserted Schmidt plot showing the general dip and trend of the S_{JO1} foliation.

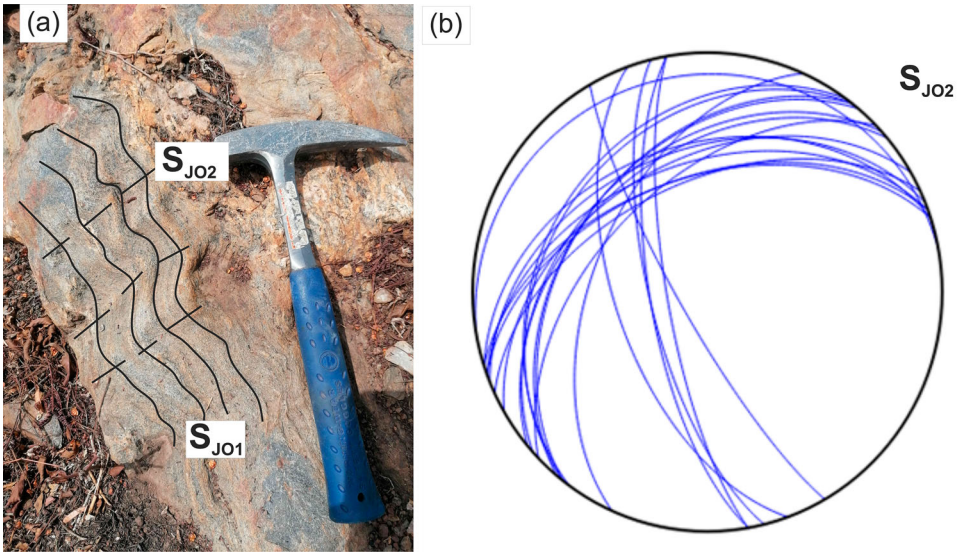

Figure 8. Field photographs and stereoplots showing structures in Josephine deposit. (a) Field photographs illustrating the relationship between S_{JO1} and S_{JO2} foliation; S_{JO2} foliation is defined by F_{JO2} open fold (b) inserted Schmidt plot showing the general dips and trend of the S_{JO2} foliations.

Isocon analysis (mass-balance considerations)

Grant (1986) developed the 'Isocon' graph as an easy solution to Gresens (1967) equation for analysing changes in volume and concentration in metasomatic alteration. This method was applied in the study of hydrothermal mineralization (Grant 1986). One can visually represent this by graphing the altered composition against the original composition, without substantial data manipulation. The 'Isocon' refers to a straight line through the origin, which represent species unaffected or immobile throughout the process. The alteration of mineralised rocks (quartzites) during the hydrothermal process was assessed by quantitatively evaluating the chemical gains and losses. This evaluation utilised whole-rock major-oxide and trace-element compositions (Table 1).

To better understand the extent of alteration, significant changes in composition, mass, and volume were assessed using the Gresens-Grant isocon approach (Gresens 1967; Grant 1986, 2005) (Figure 14). The modified EASYGRESGRANT Microsoft -Excel programme made available by Lopez-Moro (2012), updated in 2021, was employed to compare average compositions of the least altered zones with average samples from the altered zones. This approach was applied to analyse the differences between the two sets of samples. Immobile elements (e.g. zirconium (Zr), hafnium (Hf), dysprosium (Dy) and holmium (Ho)) were used as the reference frame for the analysis. The elements were chosen because it is unlikely to be mobile during hydrothermal alteration (Grant 2005).

The analysis revealed that mass was largely retained during the alteration process (Figure 14). The elements gained in the process are Au, As, Te, S, Cu, Ag, Sm, Ce and Ta. For the major oxides, Al_2O_3 and MnO were constant in the system, SiO_2, Na_2O, K_2O and CaO were added to the system, and Fe_2O_3, MgO and TiO_2, were leached from the system. Table 2 below is a summary of the chemical gains and losses in the system.

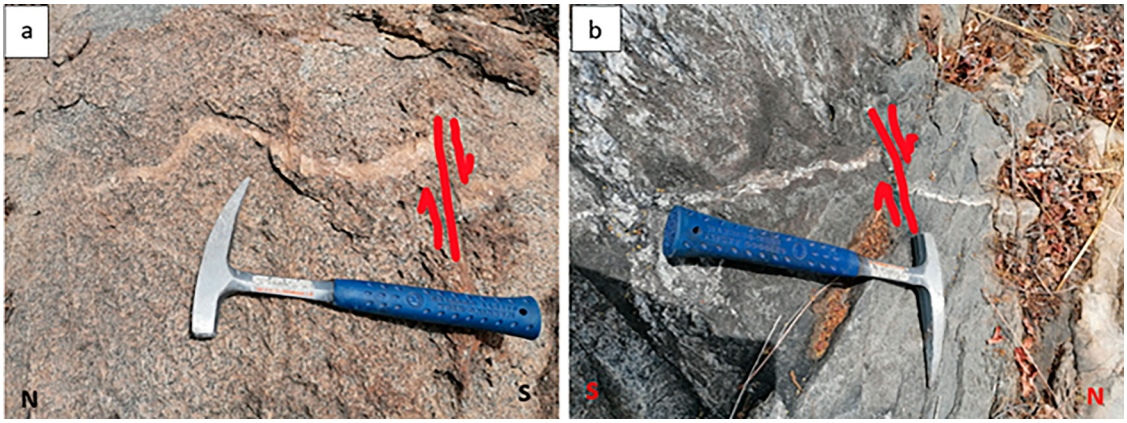

Figure 9. (a, b) Field photographs illustrating dextral faulting associated with the final stage of deformation, D_{JO3}.

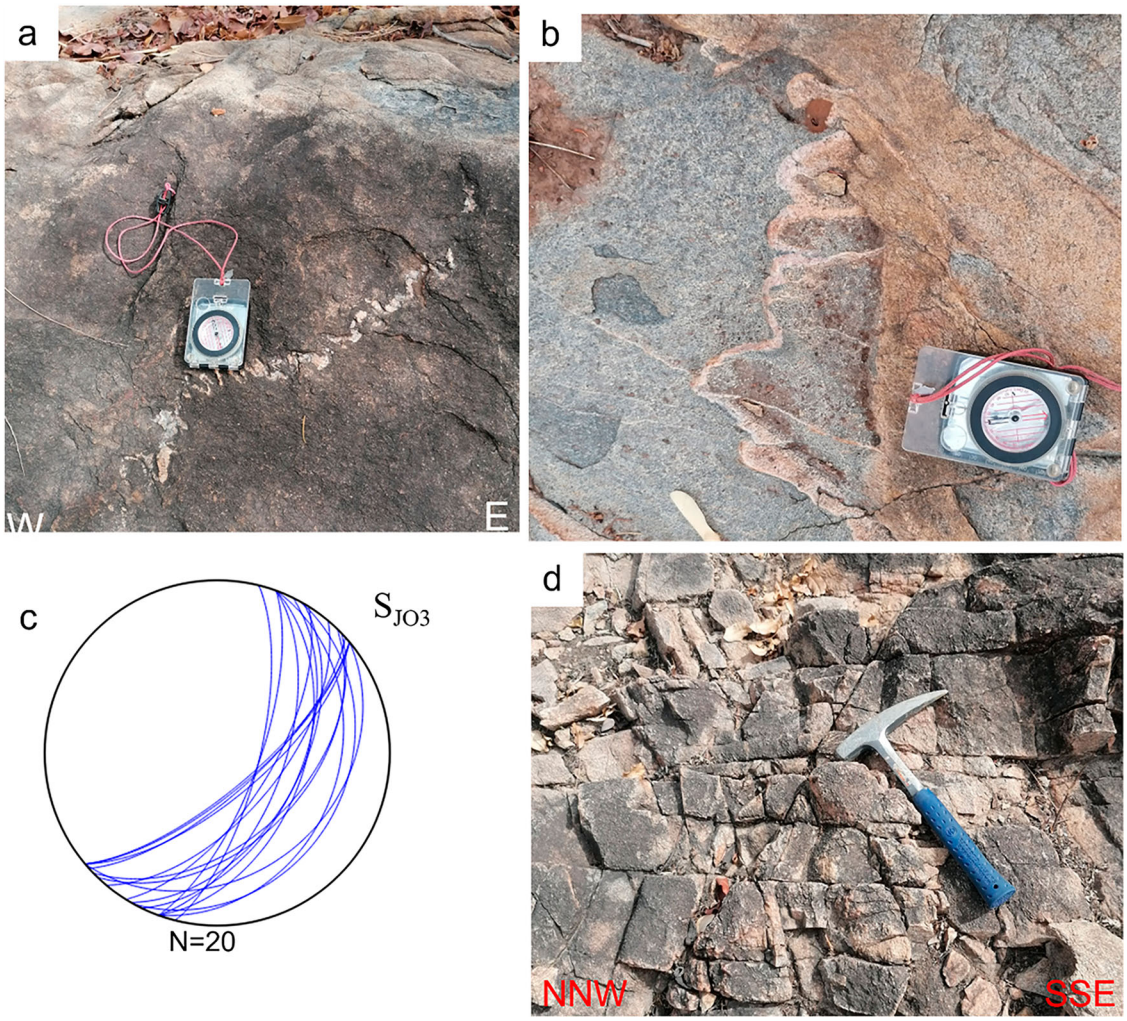

Figure 10. (a, b) Field photographs illustrating ptygmatic folding interpreted to represent the third generation of folding associated with D_{JO3} deformation, (c) inserted Schmidt plots illustrating the dip and trend of S_{JO3} foliation and (d) E-W space cleavages formed as a result of E-W directed horizontal contraction observed in the granitoid associated with D_{JO3} deformation.

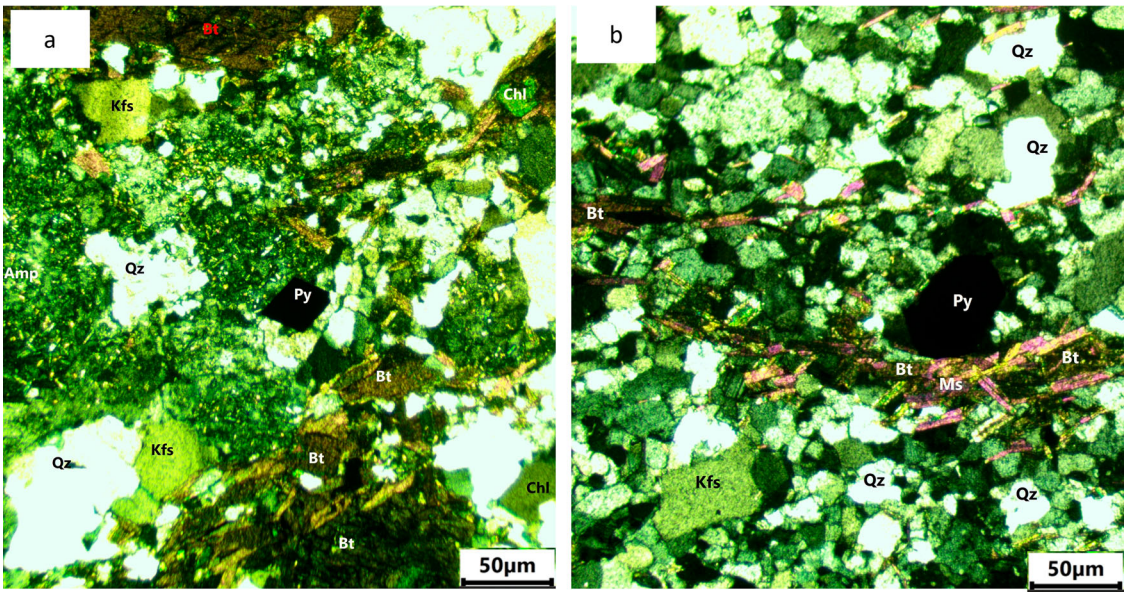

Figure 11. Photomicrograph showing the alteration mineral assemblage in the ore zone. (a) Shows the alteration mineral assemblage of quartz, chlorite and arsenopyrite with minor biotite (b) shows alteration mineral assemblage of quartz, sericite and arsenopyrite with minor micas.

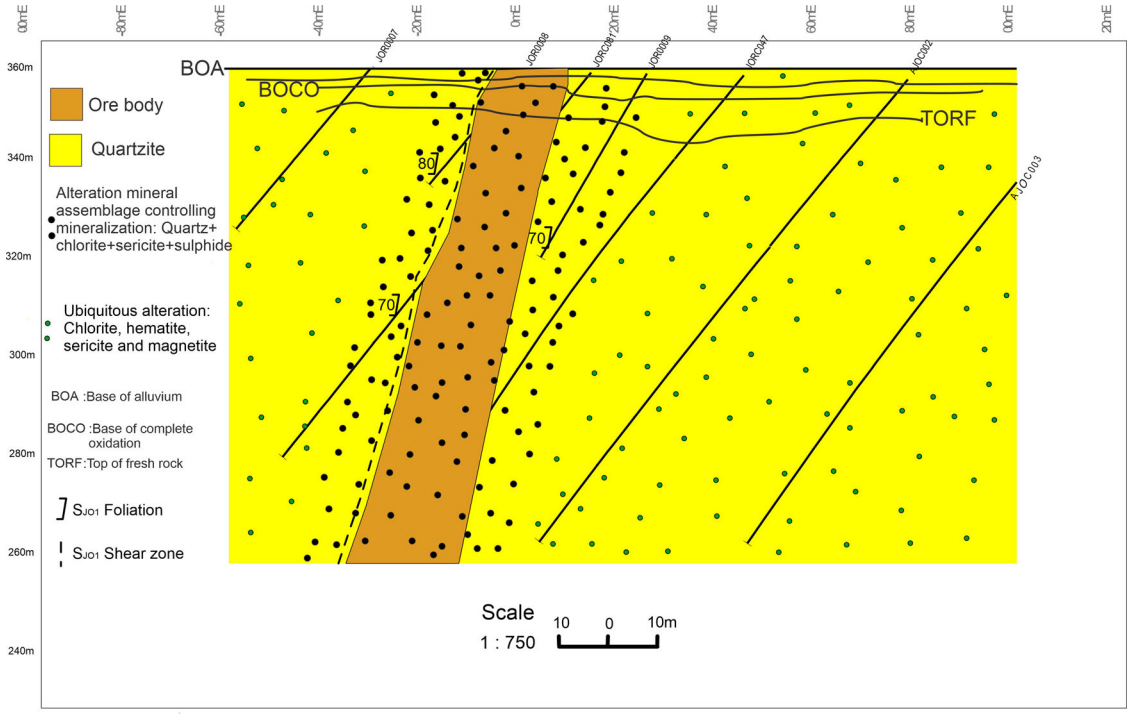

Figure 12. Cross-section (looking east) of the Josephine deposit along 576,450 mE showing the main ore body, along the NNW dextral D_{JO1} shear dipping 70°–80° NE. High-grade mineralisation is restricted to 15–40 m thick alteration zone with alteration mineral assemblage of quartz + chlorite + sericite + sulphides.

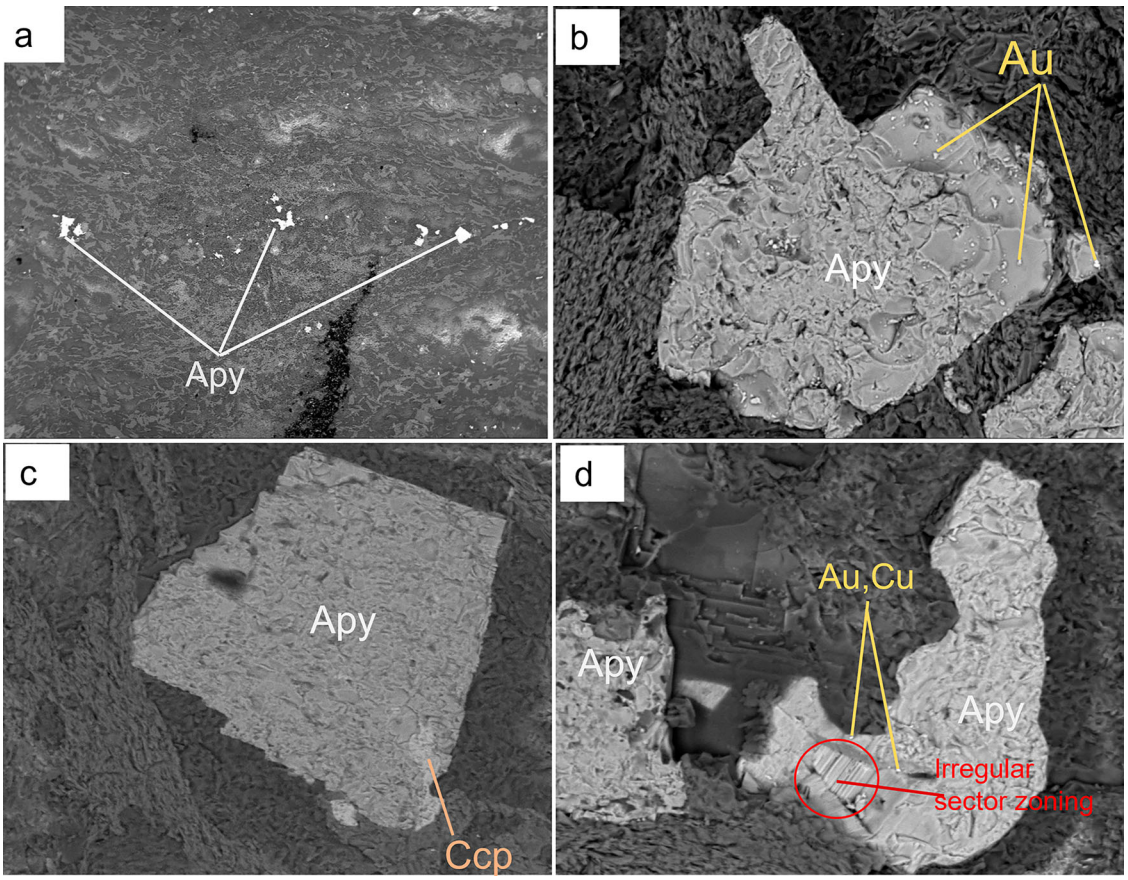

Figure 13. SEM images of arsenopyrites in the Josephine deposit (a) disseminated arsenopyrite (b) gold occurrence in arsenopyrite (c) growth of chalcopyrite on arsenopyrite and (d) irregular sector zoning in arsenopyrite. Au = gold, Cu = copper, Ccp = chalcopyrite. Mineral abbreviation is from Whitney and Evans (2010).

Table 1. Major and trace element analytical data of the mineralised quartzites in the Josephine deposit.

	Altered samples					Unaltered samples				
Sample	JO01	JO03	JO04	JO08	JO06	JO02	JO07	JO09	JO10	JO05
Wt-%										
SiO_2	60.1	69.8	59.9	72	75.9	71.5	75.5	74.9	72.4	77.9
Al_2O_3	16.35	15.45	16.2	13.2	12.65	13.95	10.7	11.95	15.3	10.55
Fe_2O_3	6.92	4.93	6.22	6.01	3.44	4.81	6.39	5.18	2.55	4.37
CaO	4.19	1.97	5.11	1.77	2.84	2.1	1.87	1.54	2.03	1.48
MgO	3.22	1.51	2.75	1.87	0.41	1.55	0.35	1.09	0.55	0.51
Na_2O	4.22	3.43	4.48	3.01	3.11	2.52	4.69	4.48	4.94	4.92
K_2O	2.81	2.75	2.16	2.08	1.04	2.61	0.99	1.44	2.65	0.54
Cr_2O_3	0.07	0.06	0.03	0.07	0.09	0.07	0.08	0.08	0.07	0.08
TiO_2	0.72	0.65	0.75	0.6	0.28	0.57	0.49	0.32	0.44	0.22
MnO	0.09	0.09	0.09	0.04	0.05	0.08	0.11	0.1	0.02	0.07
P_2O_5	0.29	0.12	0.31	0.12	0.08	0.07	0.06	0.07	0.14	0.03
SrO	0.09	0.06	0.1	0.04	0.06	0.05	0.01	0.01	0.1	0.02
BaO	0.09	0.10	0.10	0.06	0.07	0.08	0.03	0.05	0.14	0.03
LOI	2.50	1.02	1.83	1.01	1.09	0.92	0.51	0.56	0.40	0.11
Total	**101.66**	**101.94**	**100.03**	**101.88**	**101.11**	**100.88**	**101.78**	**101.77**	**101.73**	**100.83**
ppm										
Ag	1.30	0.60	0.50	1.20	0.80	0.50	0.50	0.40	0.60	0.40
As	10.50	9.62	5.60	11.00	9.82	3.62	3.10	3.82	3.62	4.10
Au	2.20	0.82	4.10	3.40	0.86	0.06	0.04	0.05	0.02	0.05
Ba	774.00	890.00	820.00	525.00	563.00	695.00	259.00	457.00	1220.00	286.00
Cd	0.40	0.40	0.50	0.50	0.40	0.50	0.50	0.30	0.50	0.40
Ce	68.50	48.00	64.80	48.90	68.00	45.50	186.00	93.10	79.70	67.50
Co	11.00	10.50	16.00	12.00	11.00	14.00	15.50	15.00	14.00	12.00
Cr	480.00	460.00	170.00	480.00	670.00	500.00	600.00	550.00	520.00	620.00
Cs	3.58	5.82	3.94	3.66	4.11	9.67	0.73	2.74	2.19	0.47
Cu	26.00	23.00	28.00	38.00	26.00	10.00	9.50	8.00	9.50	11.00
Dy	2.75	2.69	2.72	2.51	1.79	2.34	21.40	16.45	1.00	14.45
Er	1.57	1.44	1.28	1.61	0.94	1.38	13.40	11.20	0.24	8.72
Eu	1.39	1.05	1.62	1.06	1.10	0.95	2.96	2.57	1.25	2.64
Ga	20.30	17.10	19.00	13.80	14.80	13.80	20.00	24.40	20.70	18.90
Gd	3.89	3.10	4.04	3.03	2.59	2.68	19.30	14.45	2.84	13.05
Hf	3.80	5.80	3.70	4.20	2.80	3.50	19.70	11.00	5.10	10.50
Ho	0.53	0.53	0.49	0.48	0.34	0.48	4.44	3.65	0.13	2.98
La	31.10	23.20	27.90	23.40	35.00	21.10	73.70	39.10	37.30	28.10
Li	0.50	0.60	0.50	0.52	0.50	12.00	15.00	18.00	11.00	15.00
Lu	0.22	0.24	0.19	0.22	0.15	0.20	1.98	1.77	0.03	1.15
Mo	0.60	2.20	3.40	0.50	3.40	3.60	4.10	3.20	3.10	0.80
Nb	4.90	5.40	4.30	4.50	4.10	4.80	31.20	18.40	3.90	14.00
Nd	34.60	20.90	32.10	20.60	25.00	19.70	85.20	52.60	34.30	42.80
Ni	28.00	26.00	36.00	34.00	16.00	34.00	36.00	18.00	16.00	22.00
Pb	6.80	6.40	14.00	16.00	11.00	11.00	10.50	11.00	12.00	9.50
Pr	8.74	5.45	8.13	5.57	7.17	5.27	21.40	12.40	9.30	9.55
Rb	79.20	72.20	49.70	64.80	52.90	75.40	20.40	51.20	58.10	4.20
S	0.22	0.25	0.28	0.30	0.23	0.08	0.06	0.12	0.08	0.09
Sb	8.24	6.22	18.20	16.50	3.00	0.05	0.11	0.08	0.12	0.12
Sc	11.00	10.50	12.00	10.00	10.50	12.00	11.00	10.50	9.00	9.50
Se	0.82	0.62	0.48	0.42	0.42	0.44	0.46	0.45	0.46	0.45
Sm	5.86	3.89	5.97	3.79	3.97	3.73	19.30	13.35	5.16	11.40
Sn	1.00	1.00	1.00	1.00	2.00	1.00	6.00	4.00	1.00	3.00
Sr	781.00	571.00	855.00	400.00	520.00	475.00	120.00	71.00	876.00	148.50
Ta	0.30	0.40	0.20	0.30	0.40	0.30	2.00	1.20	0.20	0.90
Tb	0.50	0.44	0.50	0.43	0.33	0.41	3.28	2.50	0.25	2.23
Te	6.20	6.20	6.50	7.10	6.60	0.04	0.05	0.05	0.02	0.02
Th	1.16	5.24	1.01	3.84	6.25	3.61	8.66	4.85	2.88	1.66
Tm	0.21	0.22	0.19	0.23	0.12	0.20	2.03	1.68	0.03	1.30
U	0.28	1.56	0.44	1.23	1.63	1.30	1.88	1.50	0.85	0.53
V	144.00	115.00	112.00	118.00	73.00	89.00	25.00	20.00	36.00	19.00
W	1.00	11.00	5.00	2.00	1.00	3.00	4.00	1.00	<1	<1
Y	14.70	14.80	13.40	13.60	9.40	12.10	119.00	99.50	3.80	80.40
Yb	1.45	1.48	1.25	1.47	0.87	1.31	12.90	11.05	0.16	7.98
Zr	146.00	224.00	157.00	164.00	101.00	132.00	825.00	440.00	199.00	427.00
Zn	62.00	55.71	65.00	57.60	65.00	69.10	72.00	77.20	71.20	75.00

Discussion

Metamorphism

The principal lithologies of the Josephine gold deposit includes granitoids, quartzite, dolerite and gneiss which have undergone variable deformation and metamorphism congruent with the works of Block et al. (2015) in the Bulenga terrane and (Amponsah et al. 2015) within the Julie belt. The quartzites are intruded by granite batholiths and dolerite (Figure 15).

Metamorphism within the study area is mainly in the greenschist facies regime defined by quartz + chlorite + magnetite mineral assemblage with occurrence of micas in the quartzites, in accordance with the observation of Block et al. (2015). In the

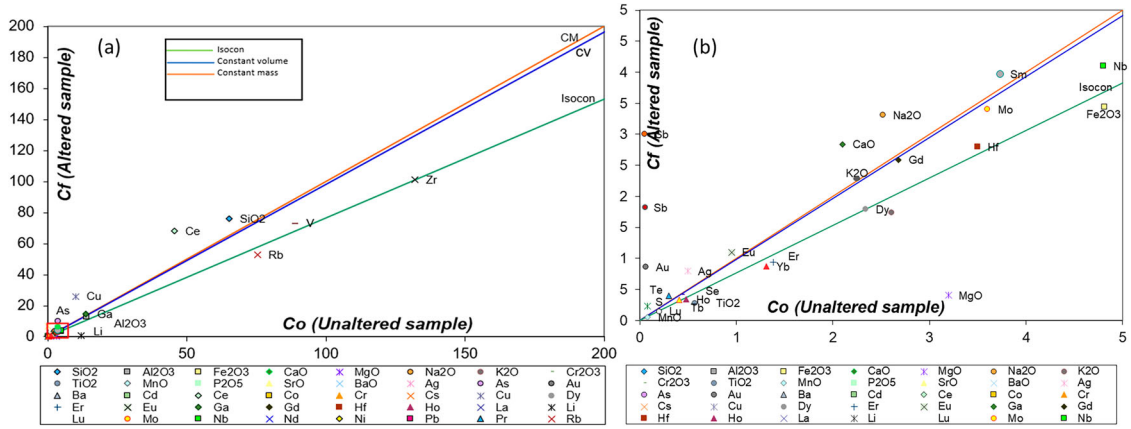

Figure 14. Isocon diagrams constructed (using the EASYGRESGRANT MS-Excel sheet in Lopez-Moro (2012); based on the theoretical development by Gresens (1967) and built upon by Grant (1986)) for five pairs each of unaltered and altered quartzites from the main ore zone. (b) Shows a close-up of the red insert in (a).

southeastern portion of the study area, amphibolite facies metamorphism is marked by the occurrence of garnet observed in the quartzites, particularly at the contacts with the granite batholith and dolerite. The mineralised quartzites in the southern part of the study area has experienced retrograde metamorphism as some of the unmineralised quartzite has garnets as a major composition.

Situating the local structure into the regional structural context

Based on the structural analysis from both field mapping and drill cores, four localised deformational regimes have been identified in the Josephine deposit, herein named as D_{JO0}, D_{JO1}, D_{JO2} and D_{JO3}. D_{JO1} which is the first episode of deformation, is noticeable by a top-to-the-NE shallow-to steeply dipping S_{JO1} penetrative shear foliation (NW-SE trending) defined by an F_{JO1} isoclinal fold and parallel to the stratigraphic layering (D_{JO0}). This deformational event correlates with the regional D_1 deformational NNE-SSW directed shortening event described by Baratoux et al. (2011) in the larger Boromo belt which also include the Wa-Lawra belt. The second deformational event (D_{JO2}) is defined by a NW-SE compression resulting into the formation of F_{JO2} folds (mostly open folds), with foliation parallel to the axial plane of the F_{JO2} folds and generally dips at an angle between 40° and 70°. It correlates with the regional D_2 described by Baratoux et al. (2011).

The final stage of deformation is the D_{JO3}. It is brittle-ductile deformation associated with an NNE-SSW S_{JO3} foliation (schistose cleavage), and dextral faulting. Folds in the form of ptygmatic folds and space cleavages, both of which formed as a result of a more E-W directed contraction was observed. This deformational regime correlates with regional D_6 and D_3 deformational event as interpretated by Block et al. (2015) for the Birimian in northwest Ghana and Baratoux et al. (2011) for the Boromo belt respectively. The shear fabrics associated with the deformation in the Josephine deposit is indicative of coaxial deformation. This means that the deformation is non-rigid and progressive (from D_{JO1} to D_{JO3}).

The brittle-ductile nature of the deformation implies that the maximum depth and temperature of deformation is about 10–25 km and 500°C respectively. Table 3 summarises the correlation between the local deformation events in the Josephine deposit and the regional events described by Block et al. (2015) and Baratoux et al. (2011).

Structural and alteration controls on gold mineralisation in the Josephine deposit

Structural controls on mineralisation

The gold mineralisation within Josephine deposit is directly associated with the shallow-to-steeply dipping dextral shear foliation (thus, the D_{JO1} deformational event). The ore zone is characterised by a shear zone which exhibit both shallow and steeply (subvertical to vertical) dipping penetrative shear fabric which gives an indication of a footwall and a hanging wall relationship. The hanging wall is defined by shallow dips and the foot wall shows steep dips in the mineralisation zone. The fault plane acts as the plumbing or fluid pathway for the gold-bearing fluid to precipitate within the shear zone.

Mineralisation within the Josephine deposit is not linked with strong veining but well associated with the alteration (silicification bleaching), however, minor veinlets observed in the mineralisation zone in rock outcrops and in drill cores are significantly mineralised. In general, the mineralised zone seems to be associated with a steeper more NNW trending zone within the generally NE-dipping sequence. This is interpreted as a right-stepping relay or sinusoidal shear bend as indicated by the shallow-to-steep dips

Table 2. Whole-rock geochemical data from the alteration zone in the quartzites used for the isocon calculations.

Alteration (mineralised zone)				Least altered	
Number of samples	5		Gain/loss in wt-% or ppm ΔCi/Co	5	
	Average (Ci_Ai)	1σ	Mass gain/loss	Average (Co)	1σ
	Mineralised			Unaltered	
Oxides (g/100g^{-1})					
SiO_2	75.90	3.20	34.11	65.10	5.53
Al_2O_3	12.65	0.12	2.58	13.95	0.20
Fe_2O_3	3.44	0.01	−0.31	4.81	0.73
CaO	2.84	0.32	1.61	2.10	0.43
MgO	0.41	0.05	−2.66	3.20	1.13
Na_2O	3.31	0.55	1.81	2.52	1.25
K_2O	2.61	0.03	0.34	1.74	1.32
Cr_2O_3	0.09	0.01	0.05	0.07	0.01
TiO_2	0.28	0.02	−0.20	0.57	0.27
MnO	0.05	0.01	−0.01	0.08	0.02
P_2O_5	0.08	0.04	0.03	0.07	0.03
SrO	0.06	0.03	0.03	0.05	0.02
BaO	0.07	0.01	0.01	0.08	0.02
Trace elements (100^{-3}g/100g^{-1})					
Ag	1.50	0.30	0.55	0.50	0.20
As	9.82	0.01	9.22	3.62	1.03
Au	3.50	0.01	1.06	0.06	0.01
Ba	563.00	16.00	40.90	695.00	54.00
Cd	0.40	0.03	0.02	0.50	0.31
Ce	68.00	4.20	43.38	45.50	7.34
Co	11.00	3.20	0.38	14.00	3.41
Cr	670.00	106.00	375.76	500.00	89.00
Cs	4.11	0.23	−4.30	9.67	1.62
Cu	26.00	2.00	23.98	10.00	3.00
Dy	1.79	0.12	0.00	2.34	0.24
Er	0.94	0.05	−0.15	1.38	0.51
Eu	1.10	0.11	0.49	0.95	0.07
Ga	14.80	2.20	5.55	13.80	3.54
Gd	2.59	1.10	0.71	2.68	1.07
Hf	2.80	0.24	0.16	3.50	1.71
Ho	0.34	0.10	−0.04	0.48	0.12
La	35.00	2.55	24.65	21.10	5.20
Li	0.50	0.00	−11.35	12.00	4.00
Lu	0.15	0.04	0.00	0.20	0.03
Mo	3.40	1.01	0.84	3.60	0.42
Nb	4.10	0.32	0.56	4.80	0.56
Nd	25.00	3.12	12.98	19.70	3.41
Ni	16.00	3.00	−13.09	34.00	6.00
Pb	11.00	2.12	3.38	11.00	2.00
Pr	7.17	1.43	4.10	5.27	0.91
Rb	52.90	5.53	−6.25	75.40	12.10
S	0.23	0.06	0.22	0.08	0.00
Sb	3.00	0.72	3.87	0.05	0.00
Sc	10.50	4.10	1.72	12.00	3.00
Se	0.42	0.08	0.11	0.44	0.04
Sm	3.97	1.30	1.46	3.73	0.14
Sn	2.00	0.63	1.61	1.00	0.00
Sr	520.00	115.70	204.69	475.00	27.00
Ta	0.40	0.01	0.22	0.30	0.04
Tb	0.33	0.00	0.02	0.41	0.02
Te	6.60	1.60	8.59	0.04	0.00
Th	6.25	0.54	4.56	3.61	0.50
Tm	0.12	0.03	−0.04	0.20	0.03
U	1.63	0.52	0.83	1.30	0.60
V	73.00	13.00	6.42	89.00	7.00
W	1.00	0.12	−1.69	3.00	1.00
Y	9.40	1.40	0.19	12.10	2.20
Yb	0.87	0.30	−0.17	1.31	0.42
Zr	101.00	9.34	0.02	132.00	29.00
Density g/cm3	3.77			3.74	

Notes: Ci_Ai = average concentration for alteration. Average of the unaltered samples segment in Table 2 was used to define the least altered sample.

in the mineralised zone. This is described as releasing bends or dilatational jogs by Groshong (1988) and Sibson (1996) respectively. This is compatible with a dextral and thrust movement sense on the Josephine fault zone. The shear deformation which resulted into brittle-ductile faulting, permitted the plumbing of the mineralising fluid, giving rise to the main dilatational structures and the resultant gold mineralisation.

Based on the ongoing discussion, it is clear that the style of gold mineralisation in the Josephine deposit is distinct from other known deposits in southern Ghana, as explained in previous studies by Allibone et al. (2004) and Feybesse et al. (2006). In those

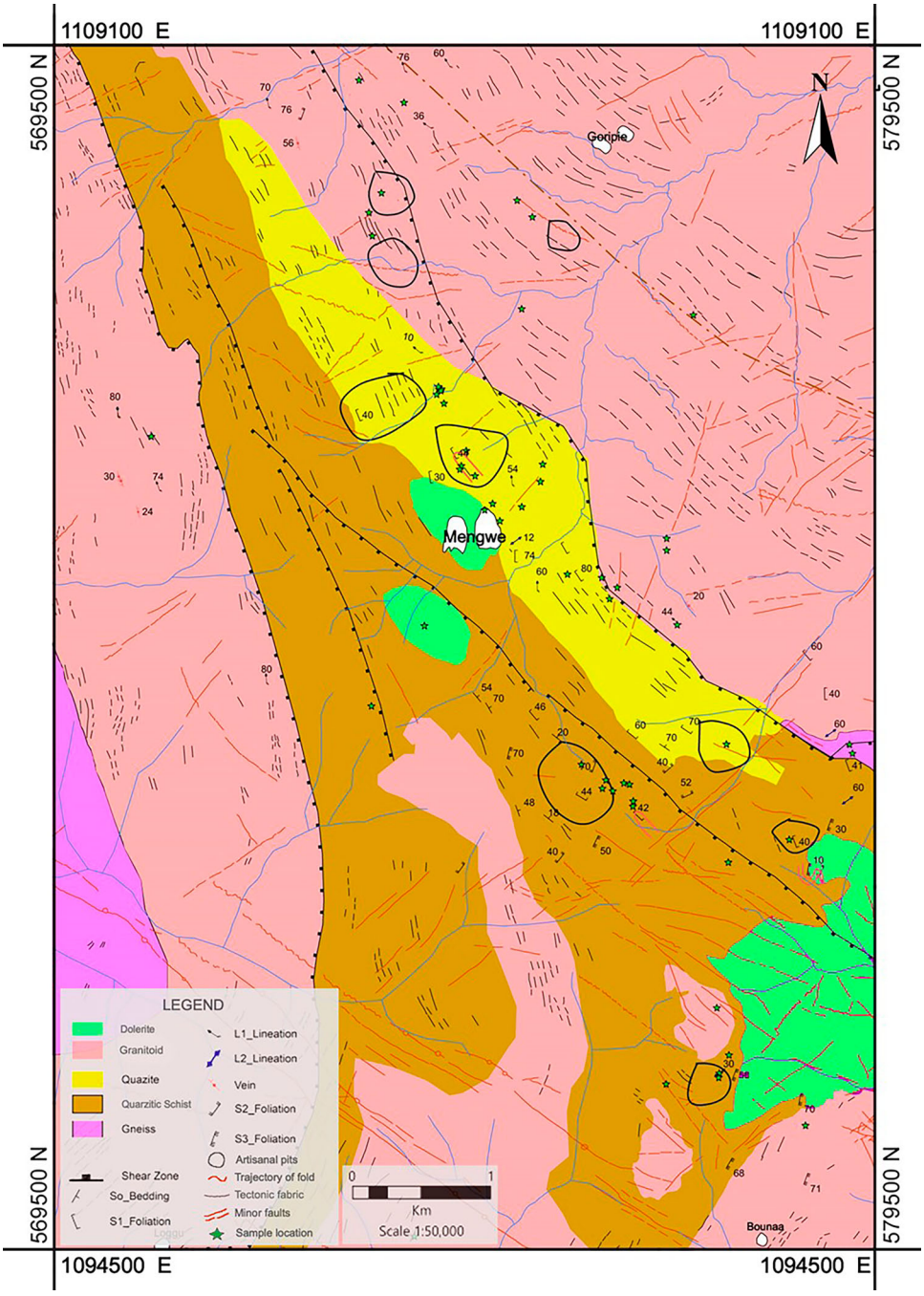

Figure 15. Simplified composite map of the Josephine deposit compiled from field data and geophysical data interpretation showing the lithological units, artisanal pits, and structures from both field measurement and geophysical data.

deposits, the formation of gold is mainly associated with the later stages of fault activity, where the faults initially moved in a reverse manner with left-lateral characteristics before experiencing brittle-ductile reactivation.

In contrast, gold mineralisation in the Josephine deposit is associated with an earlier shear zone characterised by dextral and ductile movement with reverse motion, similar to the Julie deposit interpretated by Amponsah et al. (2015).

Alteration controls on mineralisation

The quartzites in the mineralised zone have been significantly altered, with alteration mineral assemblage of recrystallized quartz, chlorite, sericite, arsenopyrite, and occasionally pyrite or chalcopyrite, or a combination of all. Chlorite and magnetite are ubiquitous in the study area, but chlorite in the mineralised zone is extremely intense.

Within the altered mineralised zone, there is a substantial replacement of magnetite by sulphides. This alteration mineralogy aligns with the greenschist metamorphic facies prevalent in the area. The geochemical variations linked to the alteration are depicted in the isocon graphs presented in Figure 11. The isocon graph reveals that the alteration process resulted in an approximate volume increase of 16.59%. Moreover, the alteration was accompanied

Table 3. Table comparing the structures observed within the Josephine deposit and that of the regional deformation sequence proposed by Block (2015) and Baratoux et al. (2011).

Study	D_1	D_2	D_3	D_4	D_5	D_6
Block (2015) NW Ghana	D1= N-S directed shortening. E-W penetrative fabric (S1) with shallow to steep dips. Low angle thrust faulting and folding	D2= N-S directed shortening. S2 foliation with moderate dips with plunging lineation down dip	D3 =E-W directed shortening and S3 schistose foliation	D4 = ENE to WSW shortening with sinistral strike slip shearing	D5= E-W brittle deformation	D6 = E-W brittle deformation, tension and brittle strike and slip fault
Baratoux et al. (2011) Boromo belt			D1 = N-NNE oriented S1 foliation. F1 fold with axial pane parallel to S1	D2 consist of steeply dipping NNE to ENE anastomosing shear zone with dextral characteristics		D3 consist of crenulation cleavages, chevron kink folds, E-W space cleavages, and the late brittle strike slip faults
Josephine Deposit			D_{JO1}= NE-SW shortening. Consist of steeply dipping NE dextral sinusoidal shear bend with S_{JO1} shear foliation and F_{JO1} isoclinal fold	D_{JO2} = NE-SW trending S_{JO2} foliation defined by F_{JO2} open folds. Lineation plunges down-dip		D_{JO3}= E-W directed shortening. Brittle-ductile deformation and S_{JO3} schistose foliation axial planar to ptygmatic folds and E-W space cleavages.

by the introduction of elements such as Au, Te, S, Cu, Ag, Sb, and Ta, indicating sulfidation, sericitization, silicification, and chloritization effects on the host rock. Additionally, variations in Ca, Si, K, Na, Fe, and Ti were observed, further supporting the influence of these alteration processes. The expected occurrence of extra silica in the mineralised area was foreseen because it indicates the introduction of quartz into the rock. It is highly probable that the leaching of iron (Fe) in the mineralised zone was a result of the significant substitution of magnetite with arsenopyrite. The addition of K in the system is as a result of the presence of sericite, an altered form of feldspars and micas. Furthermore, the Au–Sb association seen in the isocon graph is typical of orogenic Au deposits with depth of formation and temperature akin to a shallow crustal levels and relatively low temperatures (Groves et al. 1998). The significant width of the zone of alteration implies that there was circulation of fluids throughout the entire shear zone.

Based on field observations, petrographic analysis, and scanning electron microscopic (SEM) pictures of the mineralised quartzites, it was noted that the presence of gold in the Josephine deposit is linked to the formation of arsenopyrite. The existence of gold within arsenopyrite suggests that it was incorporated into the solid solution during the process of arsenopyrite precipitation. This type of association between gold and arsenopyrite has been documented in various deposits worldwide (Neumayr et al. 1993; Dalstra et al. 1997; Tarnocai et al. 1997; Genkin et al. 1998; Tomkins and Mavrogenes 2001; Yang & Zhou 2001; Morey et al. 2008; Sung et al. 2009; Fougerouse et al. 2016).

Gold in the Josephine has been identified as inclusions and free gold within arsenopyrite or occurs close to it. The small gold inclusions in arsenopyrite are most likely the result of gold co-precipitation with the sulphide (Simon et al. 1999; Reich et al. 2005).

The SEM images also shows that most arsenopyrites within the Josephine deposit display indication of As-S compositional zoning in the form of irregular sector zoning. The zoning and alteration in the sulphides indicates that they were formed during hydrothermal alteration processes.

Conclusion

Ensuing from the above discussion on the field observation, petrographic analysis, structural analysis and Isocon analysis, the following conclusion can be made on the Josephine deposit;

1. The gold mineralisation within the Josephine deposit is mainly associated with D_{JO1} deformational regime which is a steeply dipping dextral (right-stepping) relay or sinusoidal shear bend.
2. Gold occurs mostly as inclusions in the arsenopyrite mineral along S_{JO1} foliation or as free gold in the fractures of the arsenopyrites.
3. Alteration assemblage directly associated with the mineralisation zone in Josephine is quartz + chlorite + sericite + sulphide assemblages.

Acknowledgements

The authors would like to express their gratitude to Azumah Resources Limited, the owners of the Josephine deposit, for granting them access to the tenement and drill cores. Additionally, the authors would like to extend their sincere appreciation to the Agate project for providing financial

support for this research through student scholarship awards received by the first author in 2021 and 2022.

Disclosure statement

No potential conflict of interest was reported by the author(s).

Funding

Additionally, the authors would like to extend their sincere appreciation to the Agate project for providing financial support for this research through student scholarship awards received by the first author in 2021 and 2022.

ORCID

Prince Ofori Amponsah http://orcid.org/0000-0003-1349-8672

References

Abouchami W, Boher M, Michard A, Albarede F. 1990. A major 2.1 Ga event of mafic magmatism in West Africa: an early stage of crustal accretion. J Geophys Res: Solid Earth. 95(B11):17605–17629. doi:10.1029/JB095iB11p17605.

Agra NA, Elburg MA, Vorster C. 2023. Constraints on Paleoproterozoic crustal growth from Birimian Supergroup lavas of the Bui belt (Ghana) in the West African Craton. Precambrian Res. 384:106926.

Agyei Duodu J, Loh GK, Boamah KO, Baba M, Hirdes W, Toloczyki M, Davis DW. 2009. Geological map of Ghana. Vol. 1. Geological Survey Department of Ghana (GSD); p. 1000000.

Allibone A, Hayden P, Cameron G, Duku F. 2004. Paleoproterozoic gold deposits hosted by albite-and carbonate-altered tonalite in the Chirano District, Ghana, West Africa. Econ Geol. 99(3):479–497.

Amponsah PO. 2012. Multiscale structural analysis of the Sunyani Basin, Ghana [Unpublished MSc thesis]. Department of Earth Science, University of Ghana.

Amponsah PO, Forson ED. 2023. Geospatial modelling of mineral potential zones using data-driven based weighting factor and statistical index techniques. J Afr Earth Sci. 206(2023):105020. doi:10.1016/j.jafrearsci.2023.105020.

Amponsah PO, Kwayisi D, Awunyo EK, Sapah MS, Sakyi PA, Su BX, Lu Y, Nude PM. 2023. New evidence for crustal reworking and juvenile arc-magmatism during the Palaeoproterozoic Eburnean events in the Suhum Basin, South-east Ghana. Geol J. doi:10.1002/gj.4790.

Amponsah PO, Salvi S, Béziat D, Baratoux L, Siebenaller L, Jessell M, Nude PM, Gyawu AE. 2016a. Multistage gold mineralization in the Wa-Lawra greenstone belt, NW Ghana: The Bepkong deposit. J Afr Earth Sci 120:220–237. doi:10.1016/j.jafrearsci.2016.05.005.

Amponsah PO, Salvi S, Beziat D, Baratoux L, Siebenaller L, Nude PM, Nyarko RS, Jessell MW. 2016b. The Bepkong gold deposit, Northwestern Ghana. Ore Geol Rev. 78:718–732.

Amponsah PO, Salvi S, Béziat D, Siebenaller L, Baratoux L, Jessell MW. 2015. Geology and geochemistry of the shear-hosted Julie gold deposit, NW Ghana. J Afr Earth Sci. 112:505–523. doi:10.1016/j.jafrearsci.2015.06.013.

Asiedu DK, Agoe M, Amponsah PO, Nude PM, Anani CY. 2019. Geochemical constraints on provenance and source area weathering of metasedimentary rocks from the Paleoproterozoic (~ 2.1 Ga) Wa-Lawra Belt, southeastern margin of the West African Craton. Geodinamica Acta. 31(1):27–39. doi:10.1080/09853111.2019.1670414.

Augustin J, Gaboury D. 2019. Multi-stage and multi-sourced fluid and gold in the formation of orogenic gold deposits in the world-class Mana district of Burkina Faso–revealed by LA-ICP-MS analysis of pyrites and arsenopyrites. Ore Geol Rev. 104:495–521. doi:10.1016/j.oregeorev.2018.11.011.

Azumah Resources Limited. 2015. *Wa-Gold Project Internal Report*.

Azumah Resources. 2016. *Wa Gold Project internal report*.

Baratoux L, Metelka V, Naba S, Jessell MW, Grégoire M, Ganne J. 2011. Juvenile Paleoproterozoic crust evolution during the Eburnean orogeny (~ 2.2–2.0 Ga), western Burkina Faso. Precambrian Res. 191(1–2):18–45. doi:10.1016/j.precamres.2011.08.010.

Béziat D, Dubois M, Debat P, Nikiéma S, Salvi S, Tollon F. 2008. Gold metallogeny in the birimian craton of Burkina Faso (West Africa). J Afr Earth Sci. 50(2–4):215–233. doi:10.1016/j.jafrearsci.2007.09.017.

Block S. 2015. Geodynamic evolution of the West African craton in northern Ghana. Unpublished PhD thesis (University Paul Sabatier).

Block S, Ganne J, Baratoux L, Zeh A, Parra-Avila L, Jessell M, Ailleres L, Siebenaller L. 2015. Petrological and geochronological constraints on lower crust exhumation during Paleoproterozoic (Eburnean) orogeny, NW Ghana, West African Craton. J Metamorph Geol. 33(5):463–494. doi:10.1111/jmg.12129.

Block S, Jessell MW, Ailleres L, Baratoux L, Bruguier O, Zeh A, Bosch D, Caby R, Mensah E. 2016. Lower crust exhumation during Paleoproterozoic (Eburnean) orogeny, NW Ghana, West African Craton: interplay of coeval contractional deformation and extensional gravitational collapse. Precambrian Res doi:10.1016/j.precamres.2015.10.014.

Cardozo N, Allmendinger RW. 2013. Spherical projections with OSXStereonet. Comput Geosci. 51:193–205. doi:10.1016/j.cageo.2012.07.021.

Dalstra H, Bloem E, Ridley J, Groves D. 1997. Diapirism synchronous with regional deformation and gold mineralisation, a new concept for granitoid emplacement in the Southern Cross Province, Western Australia. Geol Mijnbouw. 76(4):321–338. doi:10.1023/A:1003190006222.

Davis DW, Hirdes W, Schaltegger U, Nunoo EA. 1994. U–Pb age constraints on deposition and provenance of Birimian and gold-bearing Tarkwaian sediments in Ghana, West Africa. Precambrian Res. 67:89–107. doi:10.1016/0301-9268(94)90006-X.

De Kock G, Armstrong R, Siegfried H, Thomas E. 2011. Geochronology of the Birim Supergroup of the West African craton in the Wa-Bolé region of west-central Ghana: implications for the stratigraphic framework. J Afr Earth Sci. 59(1):1–40. doi:10.1016/j.jafrearsci.2010.08.001.

Diatta F, Ndiaye PM, Diene M, Amponsah PO, Ganne J. 2017. The structural evolution of the Diale-Dalema basin, Kedougou-Kenieba Inlier, Eastern Senegal. J Afr Earth Sci. 129:923–933. doi:10.1016/j.jafrearsci.2017.02.033.

Duodu JA. 2009. Geological Map of Ghana 1: 1 000 000. Geological Survey Department.

Feng X, Wang E, Amponsah PO, Ganne J, Martin R, Jessell MW. 2019. Effect of pre-existing faults on the distribution of the lower crust exhumation under extension: numerical modelling and implications for NW Ghana. Geosci J. 23(6):961–975. doi:10.1007/s12303-019-0005-z.

Feng X, Wang E, Ganne J, Amponsah PO, Martin R. 2018. Role of volcano-sedimentary basins in the formation of greenstone-granitoid belts in the West Africa Craton: a numerical model. Minerals. 8(2):73. doi:10.3390/min8020073.

Feybesse JL, Billa M, Guerrot C, Duguey E, Lescuyer JL, Milesi JP, Bouchot V. 2006. The paleoproterozoic Ghanaian province: Geodynamic model and ore controls, including regional stress modeling. Precambrian Res. 149 (3-4):149–196.

Forson ED, Amponsah PO. 2023. Mineral prospectivity mapping over the Gomoa area of Ghana's southern Kibi-Winneba belt using support vector machine and naive bayes. J Afr Earth Sci. 206:105024. doi:10.1016/j.jafrearsci.2023.105024. in press.

Forson ED, Amponsah PO, Hagan GB, Sapah MS. 2023. Frequency ratio-based flood vulnerability modeling over the greater Accra region of Ghana. Model Earth Syst Environ. 9:2081–2100. doi: 10.1007/s40808-022-01616-y.

Forson ED, Menyeh A, Wemegah DD. 2021. Mapping lithological units, structural lineaments and alteration zones in the southern Kibi-Winneba belt of Ghana using integrated geophysical and remote sensing datasets. Ore Geol Rev. 137:104271. doi:10.1016/j.oregeorev.2021.104271.

Forson ED, Menyeh A, Wemegah DD, Danuor SK, Adjovu I, Appiah I. 2020. Mesothermal gold prospectivity mapping of the southern Kibi-Winneba belt of Ghana based on fuzzy analytical hierarchy process, concentration-area (ca) fractal model and prediction-area (pa) plot. J Appl Geophys. 174:103971. doi:10.1016/j.jappgeo.2020.103971.

Forson ED, Wemegah DD, Hagan GB, Appiah D, Addo-Wuver F, Adjovu I, Otchere FO, Mateso S, Menyeh A, Amponsah T. 2022. Data-driven multi-index overlay gold prospectivity mapping using geophysical and remote sensing datasets. J Afr Earth Sci. 190:104504. doi:10.1016/j.jafrearsci.2022.104504.

Fougerouse D, Micklethwaite S, Tomkins AG, Mei Y, Kilburn M, Guagliardo P, Fisher LA, Halfpenny A, Gee M, Paterson D. 2016. Gold remobilisation and formation of high grade ore shoots driven by dissolution-reprecipitation replacement and Ni substitution into auriferous arsenopyrite. Geochim Cosmochim Acta. 178:143–159. doi:10.1016/j.gca.2016.01.040.

Genkin AD, Bortnikov NS, Cabri LJ, Wagner F, Stanley CJ, Safonov YG, McMahon G, Friedl J, Kerzin AL, Gamyanin GN. 1998. A multidisciplinary study of invisible gold in arsenopyrite from four mesothermal gold deposits in Siberia, Russian Federation. Econ Geol. 93(4):463–487. doi:10.2113/gsecongeo.93.4.463.

Goldfarb RJ, Groves DI, Gardoll S. 2001. Orogenic gold and geologic time: a global synthesis. Ore Geol Rev. 18(1-2):1–75. doi:10.1016/S0169-1368(01)00016-6.

Grant JA. 1986. The isocon diagram; a simple solution to Gresens' equation for metasomatic alteration. Econ Geol. 81(8):1976–1982. doi:10.2113/gsecongeo.81.8.1976.

Grant JA. 2005. Isocon analysis: a brief review of the method and applications. Phys Chem Earth, Parts A/B/C. 30(17–18):997–1004. doi:10.1016/j.pce.2004.11.003.

Grenholm M, Jessell M, Thébaud N. 2019. A geodynamic model for the Paleoproterozoic (ca. 2.27–1.96 Ga) Birimian Orogen of the southern West African Craton–insights into an evolving accretionary-collisional orogenic system. Earth Sci Rev. 192:138–193. doi:10.1016/j.earscirev.2019.02.006.

Gresens RL. 1967. Composition-volume relationships of metasomatism. Chem Geol. 2:47–65. doi:10.1016/0009-2541(67)90004-6.

Groshong Jr, RH. 1988. Low-temperature deformation mechanisms and their interpretation. Geol Soc Am Bull. 100(9):1329–1360. doi:10.1130/0016-7606(1988)100<1329:LTDMAT>2.3.CO;2.

Groves DI, Goldfarb RJ, Gebre-Mariam M, Hagemann SG, Robert F. 1998. Orogenic gold deposits: a proposed classification in the context of their crustal distribution 4and relationship to other gold deposit types. Ore Geol Rev. 13(1–5):7–27. doi:10.1016/S0169-1368(97)00012-7.

Groves DI, Santosh M, Deng J, Wang Q, Yang L, Zhang L. 2020. A holistic model for the origin of orogenic gold deposits and its implications for exploration. Miner Deposita. 55(2):275–292. doi:10.1007/s00126-019-00877-5.

Hammond NQ, Robb L, Foya S, Ishiyama D. 2011. Mineralogical, fluid inclusion and stable isotope characteristics of Birimian orogenic gold mineralization at the Morila Mine, Mali, West Africa. Ore Geol Rev. 39 (4):218–229. doi:10.1016/j.oregeorev.2011.03.002.

Ibaera Capital. 2022. *Key Metrics*. https://ibaera.com/project-news/black-volta-gold-project-ghana/.

Jessell MW, Amponsah PO, Baratoux L, Asiedu DK, Loh GK, Ganne J. 2012. Crustal-scale transcurrent shearing in the paleoproterozoic Sefwi-Sunyani-Comoe region, West Africa. Precambrian Res. 212-213:155–168. doi:10.1016/j.precamres.2012.04.015.

Lawrence DM, Treloar PJ, Rankin AH, Boyce A, Harbidge P. 2013. A fluid inclusion and stable isotope study at the Loulo mining district, Mali, West Africa: Implications for multifluid sources in the generation of orogenic gold deposits. Econ Geol. 108(2):229–257. doi:10.2113/econgeo.108.2.229.

Leube A, Hirdes W, Mauer R, Kesse GO. 1990. The early Proterozoic Birimian Supergroup of Ghana and some aspects of its associated gold mineralization. Precambrian Res. 46(1-2):139–165. doi:10.1016/0301-9268(90)90070-7.

Lopez-Moro FJ. 2012. EASYGRESGRANT—a Microsoft Excel spreadsheet to quantify volume changes and to perform mass-balance modeling in metasomatic systems. Comput Geosci. 39:191–196. doi:10.1016/j.cageo.2011.07.014.

Masurel Q, Eglinger A, Thebaud N, Allibone A, Andre-Mayer AS, McFarlane H, Miller J, Jessell M, Ailleres L, Vanderhaeghe O, et al. 2022. Paleoproterozoic gold events in the southern West African craton: review and synopsis. Miner Deposita. 57(4):513–537. doi:10.1007/s00126-021-01052-5.

McFarlane HB, Ailleres L, Betts P, Ganne J, Baratoux L, Jessell MW, Block S. 2019. Episodic collisional orogenesis and lower crust exhumation during the Paleoproterozoic Eburnean Orogeny: evidence from the Sefwi Greenstone belt, West African carton. Precambrian Res. 325:88–110. doi:10.1016/j.precamres.2019.02.012.

Milési J-P, Ledru P, Feybesse J-L, Dommanget A, Marcoux E. 1992. Early Proterozoic ore deposits and tectonics of

the Birimian orogenic belt, West Africa. Precambrian Res. 58(1-4):305–344. doi:10.1016/0301-9268(92)90123-6.

Milesi JP, Feybesse JL, Pinna P, Deschamps Y, Kampunzu H, Muhongo S, Lescuyer JL, Le Goff E, Delor C, Billa M, Ralay F, Heinry C. 2004. *Geological map of Africa*. Vol. 1. SIGAfrique Project; p. 10000000. http://www.sigafrique.net.

Morey AA, Tomkins AG, Bierlein FP, Weinberg RF, Davidson GJ. 2008. Bimodal distribution of gold in pyrite and arsenopyrite: examples from the Archean Boorara and Bardoc shear systems, Yilgarn craton, Western Australia. Econ Geol. 103(3):599–614. doi:10.2113/gsecongeo.103.3.599.

Neumayr P, Cabri L, Groves D, Mikucki E, Jackman JA. 1993. The mineralogical distribution of gold and relative timing of gold mineralization in two Archean settings of high metamorphic grade in Australia. Can Mineral. 31 (3):711–725.

Nunoo S, Hofmann A, Kramers J. 2022a. Geology, zircon U-Pb dating and εHf data for the Julie greenstone belt and associated rocks in NW Ghana: implications for Birimian-to-Tarkwaian correlation and crustal evolution. J Afr Earth Sci. 186:104444. doi:10.1016/j.jafrearsci.2021.104444.

Nunoo S, Manu J, Olarewaju VO, Asiedu DK, Nude PM. 2016. Deciphering structures and deformation of the Obuom Gold Prospect, Central Ashanti Belt of Ghana: a lithostructural approach. J Afr Earth Sci. 124:159–170. doi:10.1016/j.jafrearsci.2016.09.019.

Nunoo S, Manu J, Owusu-Akyaw FK, Nyame FK. 2022b. Impact of artisanal small-scale (gold and diamond) mining activities on the Offin, Oda and Pra rivers in Southern Ghana, West Africa: a scientific response to public concern. Heliyon. 8(12):e12323. doi:10.1016/j.heliyon.2022.e12323.

Perrouty S, Allieres L, Jessell MW, Baratoux L, Bourassa Y, Crawford B. 2012. Revised Eburnean geodynamic evolution of the gold-rich southern Ashanti Belt, Ghana, with new field and geophysical evidence of pre-Tarkwaian deformations. Precambrian Res. 204–205:12–39. doi:10.1016/j.precamres.2012.01.003.

Reich M, Kesler SE, Utsunomiya S, Palenik CS, Chryssoulis SL, Ewing RC. 2005. Solubility of gold in arsenian pyrite. Geochim Cosmochim Acta. 69(11):2781–2796. doi:10.1016/j.gca.2005.01.011.

Sakyi PA, Su B-X, Anum S, Kwayisi D, Dampare SB, Anani CY, Nude PM. 2014. New zircon U–Pb ages for erratic emplacement of 2213–2130 Ma Paleoproterozoic calc-alkaline I-type granitoid rocks in the Lawra Volcanic Belt of Northwestern Ghana, West Africa. Precambrian Res. 254:149–168. doi:10.1016/j.precamres.2014.08.009.

Salvi S, Amponsah PO, Siebenaller L, Béziat D, Baratoux L, Jessell M. 2016. Shear-related gold mineralization in Northwest Ghana: the Julie deposit. Ore Geol Rev. 78:712–717. doi:10.1016/j.oregeorev.2015.08.008.

Sapah M, Agbetsoamedo JE, Amponsah PO, Dampare SB, Asiedu DK. 2020. Neodymium isotope composition of Paleoproterozoic Birimian shales from the Wa-Lawra Belt, north-west Ghana: constraints on provenance. Geol J. 56(4):2072–2081. doi:10.1002/gj.4042.

Sibson RH. 1996. Structural permeability of fluid-driven fault-fracture meshes. J Struct Geol. 18(8):1031–1042. doi:10.1016/0191-8141(96)00032-6.

Simon G, Huang H, Penner-Hahn JE, Kesler SE, Kao L-S. 1999. Oxidation state of gold and arsenic in gold-bearing arsenian pyrite. Am Mineral. 84(7–8):1071–1079. doi:10.2138/am-1999-7-809.

Sung Y-H, Brugger J, Ciobanu C, Pring A, Skinner W, Nugus M. 2009. Invisible gold in arsenian pyrite and arsenopyrite from a multistage Archaean gold deposit: Sunrise Dam, Eastern Goldfields Province, Western Australia. Miner Deposita. 44(7):765–791. doi:10.1007/s00126-009-0244-4.

Tarnocai CA, Hattori K, Cabri LJ. 1997. "Invisible" gold in sulfides from Campbell Mine, Red lake greenstone belt, Ontario; evidence for mineralization during the peak of metamorphism. Can Mineral. 35(4):805–815.

Tomkins AG, Mavrogenes JA. 2001. Redistribution of gold within arsenopyrite and lollingite during pro-and retrograde metamorphism: application to timing of mineralization. Econ Geol. 96(3):525–534. doi:10.2113/gsecongeo.96.3.525.

Tourigny G, Tranos MD, Masurel Q, Kreuzer O, Brammer S, Owusu-Ansah K, Yao D, Hayford T. 2019. Structural controls on granitoid-hosted gold mineralization and paleostress history of the Edikan gold deposits, Kumasi Basin, southwestern Ghana. Miner Deposita. 54 (7):1033–1052. doi:10.1007/s00126-018-0858-5.

Treloar P, Lawrence D, Senghor D, Boyce A, Harbidge P. 2015. The Massawa gold deposit, eastern Senegal, West Africa: an orogenic gold deposit sourced from magmatically derived fluids? Geol Soc Lond Spec Publ. 393 (1):135–160. doi:10.1144/SP393.12.

Whitney DL, Evans BW. 2010. Abbreviations for names of rock-forming minerals. Amer Min. 95(1):185–187.

Yang J-H, Zhou X-H. 2001. Rb-Sr, Sm-Nd, and Pb isotope systematics of pyrite: implications for the age and genesis of lode gold deposits. Geology. 29(8):711–714. doi:10.1130/0091-7613(2001)029<0711:RSSNAP>2.0.CO;2